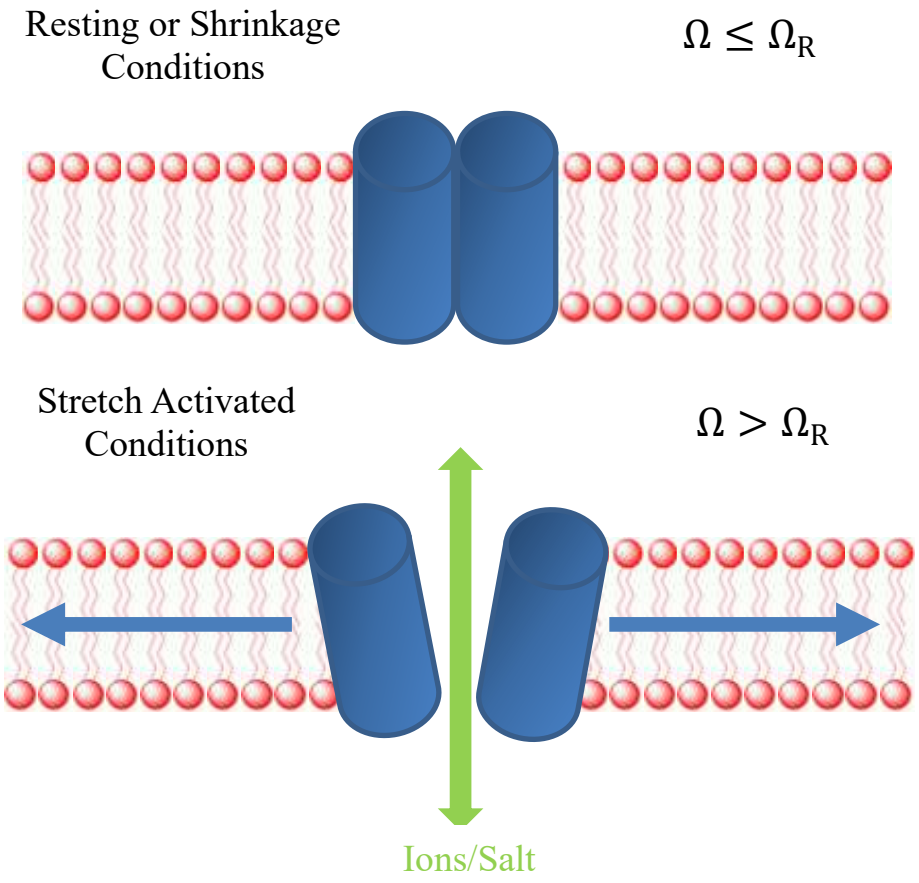
Resting or Shrinkage Conditions
$\Omega \leq \Omega_R$
Stretch Activated Conditions
$\Omega > \Omega_R$
Ions/Salt

- Modeling of the non-perfect osmometer behavior of animal cells for cryopreservation.
- Comparison with the two-parameter formalism: differences and analogies.
- Validity of the equilibrium equations for non-perfect osmometer cells.
- Parametric sweep analysis.

Insights into the model of non-perfect osmometer cells for cryopreservation: a parametric sweep analysis

Gabriele Traversari and Alberto Cincotti*

Dipartimento di Ingegneria Meccanica, Chimica e dei Materiali, Facoltà di Ingegneria e Architettura, Università degli Studi di Cagliari, Via Marengo 2, 09123, Cagliari, Italy

* Author to whom correspondence should be addressed (email: alberto.cincotti@dimcm.unica.it)

Keywords: Osmosis; Mechanosensitive ion channels; Surface area regulation; Parametric sweep; Cryopreservation

Insights into the model of non-perfect osmometer cells for cryopreservation: a parametric sweep analysis

Gabriele Traversari and Alberto Cincotti*

Dipartimento di Ingegneria Meccanica, Chimica e dei Materiali, Facoltà di Ingegneria e Architettura, Università degli Studi di Cagliari, Via Marengo 2, 09123, Cagliari, Italy

* Author to whom correspondence should be addressed (email: alberto.cincotti@dimcm.unica.it)

Keywords: Osmosis; Mechanosensitive ion channels; Surface area regulation; Parametric sweep; Cryopreservation

November 2020

Abstract

Recently, a mathematical model able to describe the non-perfect osmotic behavior of cells during cryopreservation was proposed. The model improves the two-parameter formalism typically adopted in cryopreservation literature by allowing the transmembrane permeation of ions/salt, through the temporary opening of mechanosensitive channels whenever membrane stretching occurs: cells can reach an equilibrium volume different from the initial one, when isotonic conditions are re-established after contacting with impermeant or permeant solutes, such as sucrose or a cryoprotectant agent like dimethyl sulfoxide, respectively.

Although the model was conceived as a conservative development of the two-parameter formalism to avoid over-parameterization, a complex picture of the system emerges. To describe this, first an appropriate non-dimensional version of the model equations is derived. Then, a parametric sweep analysis is performed and discussed to highlight the features of the novel model in comparison with the two-parameter formalism: the conditions by which the first reduces to the second are identified. Only equilibrium equations with impermeant sucrose may be analytically derived from the model: their validity is here extended much more than originally assumed. When permeant dimethyl sulfoxide comes into play, the temporary opening of mechanosensitive channels is difficult to predict and prevents the derivation of the equilibrium equations: in this case, a numerical integration of system dynamics up to steady state is required to determine the cell volume at equilibrium. In conclusion, cell volume at equilibrium depends on the position of the temporal window of mechanosensitive channels opening, which, in general, is a complex function of model parameters and operating conditions.

Introduction

Nowadays, cells are mainly conserved by means of cryopreservation, that is by maintaining at sub-zero temperatures. Usually, this process consists of a sequence of different steps sometimes in combination: osmotic addition of a permeant cryoprotectant agent (CPA) like dimethyl sulfoxide (DMSO), cooling, storage, thawing, and CPA removal. Several phenomena are involved, including cell osmotic response to the contact with CPAs and their possible cytotoxicity, and intracellular ice or glass formation and disappearance. Often an unacceptable decrease in cell viability and functionality results [16,24], due to the physico-chemical and biological changes cells are subjected to. Thus, optimization of the operating conditions adapted to the osmotic behavior of the specific cell lineage under investigation is crucial for cryopreservation. However, the number of experimental variables and parameters is prohibitively large to permit a rigorous optimization of cryopreservation procedures [5,17]. On the other hand, best practices may be defined through mathematical modelling and numerical simulations [7-11,16]. At least, this allows to identify the most influential factors and reduce the experimental efforts, provided that the adopted mathematical model is valid and capable to describe the behavior of the system.

In the field of cryopreservation, the two-parameter formalism [20] is the mathematical model typically adopted to interpret the osmotic behaviour of cells during CPA addition and removal. One of its basic assumptions is that the content of intracellular solutes responsible for the isotonic osmolality remains constant with time, i.e. they are impermeant through the cell membrane. On the contrary, water and permeant CPAs may passively diffuse through the cell membrane, exchanged between ideal liquid solutions. This is the perfect osmometer behaviour, the main consequence of which is that, at isotonic conditions, cells necessarily return to their original isotonic volume, regardless of the followed osmotic path and volume excursion. The locus of equilibrium cell volume is the so-called Boyle Van't Hoff plot, whose linearity is a reflection of the perfect osmometer behaviour.

Recently, our experiments demonstrated that human mesenchymal stem cells (hMSCs) from umbilical cord blood (UCB) do not behave as perfect osmometers [3-4]: positive cell volume excursions are limited during DMSO addition and removal (from here on called the osmotic cycle with DMSO), and the restoration of isotonic conditions after the contact with hypertonic solutions of impermeant solutes (from here on called the

osmotic cycle with sucrose). In particular, when restoring the isotonic conditions, the cell volume attains a final, equilibrium value that is different from the initial, isotonic one, and depends on system temperature.

To follow this osmotic behavior with the classic two-parameter model, an iterative fitting of data would be required, with model parameters left free to vary depending on operating conditions, while they are expected to remain constant [3-4]. Besides, removing the assumption of ideal, dilute solutions thus following the approach developed by Elliott and co-workers [25-26], would not solve the problem: with the thermodynamics of non-ideal solutions embedded into the two-parameter formalism, cells would keep returning to isotonic osmolality and to their original isotonic volume when isotonic conditions are re-established after an osmotic cycle with sucrose or DMSO, albeit not in a completely linear fashion in the Boyle Van't Hoff plot. Similarly, by accounting for the concentration dependence of the cell permeability to cryoprotectant and water in the framework of the two-parameter model, only the kinetics followed in the osmotic excursion would be affected. In fact, a slower osmotic response was observed for red blood cells when working at higher concentrations [1,2,12,28,29,31] so that both water and CPA permeability were simulated as decreasing when solution osmolality increases [22,23]; other authors working on mouse oocytes found that water and CPA permeability increase with solution osmolality [6,13], whereas in the porcine oocyte system the dependence of cell membrane permeability was extended to include also the hydration level and absence or presence of ice [32]. However, regardless of the specific functional dependence adopted, with this kind of model improvement of the two-parameter formalism the cell volume reached at equilibrium when isotonic conditions are re-established after an osmotic cycle with DMSO or sucrose would not change, and the return to the initial, isotonic cell volume would be simulated anyway.

On the other hand, a much more complex picture than the one depicted by the two-parameter model typically used in cryopreservation emerges from the biophysics and physiology literature addressing the control of cell volume and shape [21,30]: the osmotic response of a cell population, and the regulation of its surface area with membrane folds and blebs by means of exo- and endo-cytosis is the result of the combined effect of mechanics, electrical and chemical potentials. Unfortunately, a quantitative understanding of the whole picture is still lacking, and a general model embedding all these phenomena is not yet available. On the other hand, a comprehensive mechanistic model may prove to be over-parameterized, which may preclude its validation and a reliable determination of all its parameters.

For these reasons, we recently proposed a novel mathematical model [5] from here on named the SAR model, where osmosis is coupled with cell mechanics and cell membrane surface area regulation: now solute (ions/salt) permeation through the temporary opening of mechanosensitive (MS) channels is allowed, when the cell membrane is stretched. This way cells can reach an equilibrium volume different from the initial isotonic one, when isotonic conditions are re-established after an osmotic cycle with sucrose or DMSO. The choice to address the trans-membrane exchange of electro-neutral chemical species as ions/salt was made on purpose in order to avoid the description of the coupling between electro-magnetic field and mass diffusion used in the well-known pump and leak physiological model (PLM) [18-19]. On the other hand, the PLM involves active mechanisms such as ion pumps which consume energy. For this reason, these mechanisms are considered only for long-term regulation of cell volume but are typically neglected in cryopreservation where only relatively short-term responses are taken into account. By means of the SAR model, a successful description of the non-perfect osmotic behaviour measured for hMSCs from UCB was possible: unknown model parameters were determined through a best fit procedure, and full predictions of non-fitted data were provided to validate the model [5].

The SAR model was conceived as a conservative development of the two-parameter formalism explicitly to avoid over-parameterization: the simplifying assumption of ideal liquid solutions is maintained, but the description of transport mechanisms is enriched by accounting for three additional phenomena (namely ion/salt conditional permeation, membrane surface area regulation, and counter-gradient of hydrostatic pressure to osmosis), thus introducing five additional parameters (i.e. membrane resting tension, thickness and elastic modulus, ion/salt permeability, and membrane relaxation rate constant). Nonetheless, a complex picture of the system results as it will be shown in this work: depending on the relative values of the model parameters and operating conditions, when isotonic conditions are re-established after any osmotic excursion where the cell membrane is stretched, cell volume at equilibrium depends on the position of the temporal window of mechano-sensitive channels opening.

In this work, first an appropriate non-dimensional version of the equations for the SAR model is derived, in order to minimize the number of model parameters. Then, a parametric sweep analysis is discussed to highlight model features in comparison with the two-parameter model, that basically represents a special case of the SAR model. Regarding this, the conditions in terms of the values of the adjustable parameters by

which the SAR model reduces to the two-parameter model are identified. Besides, only equilibrium equations after an osmotic cycle with impermeant sucrose may be analytically derived for the SAR model, albeit without the advantageous linearity of the Boyle Van't Hoff equation. It is shown that, the validity of these equilibrium conditions with respect to the values of the adjustable parameters may be generalized and extended much more than originally assumed in [5]. On the contrary, when a permeant CPA comes into play the difficulty to predict the temporary opening of MS channels prevents the derivation of the corresponding equilibrium equations: in this case, a numerical integration of system dynamics (prolonged until steady state is eventually reached) is required to determine cell volume at equilibrium.

Model Equations

Dynamics

Starting from the model equations in dimensional form reported in our previous paper [5], in this work the corresponding non-dimensional equations are derived by defining a reference, constant value to scale all the variables. The resulting equations in non-dimensional form are collectively reported in Tables 1-2, with Ordinary Differential Equations (ODEs) conveniently separated by auxiliary Algebraic Equations (AEs). The procedure of non-dimensionalization is detailed in the appendix section. It is worth noting that the non-dimensional time ($\tau = \frac{t}{t^*}$) is defined with respect to a reference value based on water permeability and depends on temperature $\left(t^* = \frac{\left(\frac{3}{4\pi} V_{\mathrm{Cell}}^0\right)^{\frac{1}{3}}}{3\, L_{\mathrm{P}}(T)\, R\, T\, \mathrm{M}^0} \right)$. As a consequence, in this work system temperature is assumed constant during any simulation. Moreover, in the adopted non-dimensionalization each dimensional variable or parameter uniquely corresponds to a non-dimensional one. Thus, from here on every variable or parameter is called with its generic name without specifying to refer to dimensional or the non-dimensional one, unless necessary.

A thorough discussion of the equations of the SAR model with its development is available in the literature [5] and it is not repeated in this work, where only the following brief description is provided.

In contrast with the classic two-parameter model, the SAR model allows the trans-membrane exchange of the solutes responsible of the initial isotonic osmolality, identified as ions as schematically depicted in Figure

1. Here the inactive (υ_{B}), water (ζ_{W}), CPA (ζ_{CPA}) and ion (ζ_{Ions}) volume fractions contribute to form the cell volume (ζ_{Cell}), as defined by Equation 5 in Table 2. Except for the inactive volume and any impermeant solutes like sucrose, in the SAR model water and CPA as well as ion may be exchanged between intra- and extra-cellular compartments as expressed by Equations 1-3 in Table 1, respectively. Here the non-dimensional kinetic parameters like ion and CPA permeability (λ_{Ions} and λ_{CPA}) are defined with respect to water permeability (L_{P}). In particular, a conditional ion exchange represented by Equation 3 is considered as expressed by Equation 17, depending on the opening of MS channels. These are assumed to be distributed all over the cell membrane, the spherical surface area (Φ_{Sph}) of which varies in time as cells shrink or swell (see Equation 9); MS channels open when the cell membrane is mechanically stretched above its resting tension (i.e. $\Omega > \Omega_{\mathrm{R}}$ or $\Delta\Omega > 0$). This stretching of the cell membrane surface area (Φ_{Sph}) is measured by the surface strain from its reference value (Φ_{Ref}) as defined by Equations 7-8, and is only temporary: membrane relaxation through the exchange of surface area with membrane reservoirs is able to bring cell back to the resting condition by following Equation 4, where the non-dimensional kinetic parameter (λ_{S}) is also defined with respect to water permeability (L_{P}).

Basically, in the SAR model a cell under isotonic conditions is seen as an inflatable balloon whose surface Φ_{Sph} is initially stretched from Φ_{Ref} at a resting tension Ω_{R} representing homeostatic condition, as expressed by the initial condition of Equation 4. In response to an osmotic gradient $\Delta\omega$ between intra- and extra-cellular compartments expressed by Equations 10-16, the cell inflates or deflates (through the exchange of water, CPA, and ions) by changing its spherical volume ζ_{Cell} and its membrane surface area Φ_{Sph}. As a consequence, the ratio $\frac{\Phi_{\mathrm{Sph}}}{\Phi_{\mathrm{Ref}}}$ varies from its value at resting condition ($1 + \frac{\Omega_{\mathrm{R}}}{K'}$) in a proportional fashion with cell membrane tension Ω, i.e. an elastic response from a mechanical perspective, with K' representing the non-dimensional elastic modulus defined in Equation 8. This variation has two consequences: according to the Laplace law (i.e. Equation 6) a counter-gradient of hydrostatic pressure $\Delta\mathrm{p}$ always opposing the osmotic driving force $\Delta\omega$ in the water exchange rate emerges (note the opposite signs of the two driving forces in Equation 1), while MS channels open allowing ion exchange (inward or outward depending on their gradient) if the membrane is stretched, i.e. if $\Omega > \Omega_{\mathrm{R}}$ or $\left(\frac{\Phi_{\mathrm{Sph}}}{\Phi_{\mathrm{Ref}}}\right) > \left(1 + \frac{\Omega_{\mathrm{R}}}{K'}\right)$. On the other hand, the variation of membrane tension with respect to the resting condition is only temporary due to membrane relaxation

governed by Equation 4: it eventually vanishes through the exchange of surface area with membrane reservoirs, which brings the membrane tension back to its resting value in order to maintain cell homeostasis. The exchange rates reported in Table 1 are all determined as proportional to the product of a flux represented by a driving force and the corresponding cross-sectional area, with non-dimensional ions and CPA permeability (λ_{Ions}, λ_{CPA}) as well as λ_{S} being the constants of proportionality. For water, CPA and ion exchange rates the cross-sectional area is represented by the spherical cell membrane area Φ_{Sph} in Equations 1-3, while in the membrane generation/relaxation rate expressed by Equation 4 Φ_{Ref} is multiplied with the driving force $\Delta\Omega$ for the exchange flux of lipid bilayer with membrane reservoirs.

The two-parameter model in non-dimensional form consists of a subset of the equations reported in Tables 1-2 for the SAR model, namely Equation 1 (with $\Delta\mathrm{p} = 0$) and Equation 2 for the ODE system shown in Table 1 where the content of intracellular ions is kept constant at its initial value (i.e. initial condition of Equation 3), along with Equations 5, 9-15 for the auxiliary AEs system reported in Table 2. Basically, with respect to the two-parameter formalism the SAR model introduces three additional phenomena (ion permeation, membrane surface area regulation, and counter-gradient of hydrostatic pressure to osmosis) along with five adjustable non-dimensional parameters (cell membrane resting tension Ω_{R}, thickness β and elastic modulus K', ion/salt permeability λ_{Ions}, and membrane relaxation rate constant λ_{S}). Since in the SAR model ion permeation depends on the opening of MS channels whose duration is governed by the rate of membrane relaxation which, in turn, is triggered by osmosis, a much more complex picture than in the two-parameter model is depicted, where all phenomena are strictly interrelated and affect each other.

Equilibrium with impermeant solutes

Cell volume ζ_{Cell} at osmotic equilibrium can be determined by solving model equations in Tables 1-2 at steady state. If a permeant CPA is absent, in the osmotic cycle with impermeant sucrose steady state is reached when the driving forces appearing in Equations 1, 3 and 4 for the exchange rate of water, ions and membrane reference surface are equal to zero. Assuming $\Delta\mathrm{p} \ll \Delta\omega$ and λ_{S} is small (so that membrane relaxation is relatively slow and MS channels remain open during swelling), it was possible to derive the equations reported in Table 3 for the cell volume at equilibrium. More specifically, in Equations 18-19 the

equilibrium value of cell volume after an osmotic cycle with impermeant sucrose in the absence of CPA and with $\omega^{\mathrm{EXT,\,II}} \leq \omega^{\mathrm{EXT,\,I}}$ is reported: during phase I, cells first shrink due to the contact with hypertonic solutions of sucrose and ions ($\omega^{\mathrm{EXT,\,I}} = \omega_{\mathrm{Sucrose}}^{\mathrm{EXT,\,I}} + \omega_{\mathrm{Ions}}^{\mathrm{EXT,\,I}}$), then swell back when removing sucrose in phase II by contacting with relatively hypotonic solutions made only of ions, without sucrose ($\omega^{\mathrm{EXT,\,II}} = \omega_{\mathrm{Ions}}^{\mathrm{EXT,\,II}}$). It is worth noting that a complete mechanical relaxation of membrane tension is assumed to be reached at the end of phase I, before phase II starts. The detailed derivation of these equations may be found in [5]. In Table 3 the contributions of water and ions to cell volume are highlighted. Note that $\mu_{\mathrm{Ions}} = \frac{\tilde{v}_{\mathrm{Ions}}\, M^0}{\varphi}$ represents the ratio between the intracellular ion and water volumes at isotonic conditions: it is a very small number which is typically neglected in the two-parameter model.

During phase I, isotonic cells shrink, no ion exchange takes place since membrane tension is always lower than the resting value and MS channels remain closed. Thus, the classic Boyle Van't Hoff equation (i.e. Equation 18) resulting from the two-parameter model is derived also from the SAR model: a linear dependence between the cell volume at equilibrium ($\zeta_{\mathrm{Cell}}^{\mathrm{I}}$) and the inverse of the external osmolality ($\frac{1}{\omega^{\mathrm{EXT,\,I}}}$) allows the inactive volume fraction, v_B, to be determined through a simple linear regression. Besides, this Boyle Van't Hoff equation does not depend on temperature, and predicts a perfect osmometer behavior, that is $\zeta_{\mathrm{Cell}}^{\mathrm{II}} = 1$ when the isotonic conditions are re-established in phase II by setting $\omega^{\mathrm{EXT,\,II}} = 1$.

On the contrary, during the swelling in phase II in the SAR model cell membrane is stretched and reaches tensions above Ω_{R} which leads to MS channels opening and leakage of intracellular ions: now the cell volume at equilibrium is given by Equation 19. More specifically, the deviation from the Boyle Van't Hoff equation is represented by the term $\left(\frac{\mu_{\mathrm{Ions}} + \frac{\lambda_{\mathrm{Ions}}}{\omega^{\mathrm{EXT,\,I}}}}{\mu_{\mathrm{Ions}} + \frac{\lambda_{\mathrm{Ions}}}{\omega^{\mathrm{EXT,\,II}}}}\right)$ (cf. with Equation 18), and it clearly depends on λ_{Ions}: now the linear profile of cell volume ($\zeta_{\mathrm{Cell}}^{\mathrm{II}}$) vs the reciprocal of external osmolality ($\frac{1}{\omega^{\mathrm{EXT,\,II}}}$) is lost, that is a non-perfect osmometer behavior results. It should be noted that, Equation 19 reduces to the Boyle Van't Hoff equation when $\lambda_{\mathrm{Ions}} = 0$: in such a case no leakage of ions may actually take place since ion permeability is zero, and the new model reduces to the two-parameter model at equilibrium. Moreover, since $\lambda_{\mathrm{Ions}}(\mathrm{T})$ shows an Arrhenius-like dependence, Equation 19 predicts a partial recovery of the isotonic cell volume that depends on system temperature.

Model Parameters

Through a sequential best fit procedure involving equilibrium as well as dynamic runs of hMSCs from UCB with DMSO or sucrose at varying osmolalities and temperatures, all the unknown model parameters were determined [5]. More specifically, the values of the dimensional parameters were determined through a series of regression steps characterised by a progressive increase of model complexity: first, determine only the inactive volume fraction v_B from equilibrium runs in hypertonic solutions with sucrose at different osmolalities, but at constant temperature (see Figure 4 in [5]); then, with v_B kept constant at the value just estimated, determine water and ion permeability with their Arrhenius-like temperature dependence ($L_P(T)$ and $P_{Ions}(T)$), and membrane relaxation rate constant (k_S) from the dynamic runs of the osmotic cycle with sucrose at constant osmolality, but at three different temperatures (see Figure 5 in [5]); finally, keeping all the previous parameters constant, determine CPA permeability and its Arrhenius-like temperature dependence (P_{CPA}(T)) from the dynamic runs of the osmotic cycle with DMSO at constant osmolality, but three different temperatures (see Figure 6 in [5]). At last, the predictive capability of the proposed model was validated using test data from experimental runs performed under transient conditions when contacting cells with hypertonic solutions of DMSO at two different osmolalities but at constant temperature (see Figure 7 in [5]), and data from two consecutive osmotic cycles with sucrose at constant osmolality and temperature (see Figure 8 in [5]).

The corresponding values of the model parameters in non-dimensional form at room temperature are reported in Table 4. This represents the base case of the *one factor at time* parametric sweep analysis performed in this work, where every non-dimensional parameter is varied individually except for μ_{CPA}, μ_{Ions} and v_B that are kept constant. At first glance, based on the values of the kinetic parameters (cf. λ_S, λ_{CPA}, and λ_{Ions}) shown in Table 1, in the base case membrane relaxation should be the fastest phenomenon with respect to water permeation, while ion exchange should represent the slowest one.

Results and discussion

To the best of our knowledge, the SAR model is the first and only mathematical model available in the literature of cryopreservation addressing the behavior of non-perfect osmometer cells that do not return back to their initial volume when isotonic conditions are re-established after an osmotic excursion. In this work, a parametric sweep analysis is used to discuss model features in comparison with the two-parameter model. For the sake of clarity, this analysis is carried out by simulating the osmotic cycle with impermeant sucrose in the absence of permeant DMSO and vice versa.

Osmotic cycle with impermeant sucrose in the absence of permeant DMSO

The case of cells put in contact with sucrose is examined first. More specifically, isotonic cells are suspended in a hypertonic solution of sucrose added to isotonic ions (like PBS) in the shrinking phase I (i.e. $\omega_{\mathrm{Sucrose}}^{\mathrm{EXT,I}} = 1$, $\omega_{\mathrm{Ions}}^{\mathrm{EXT,I}} = 1$), before returning back to isotonic conditions when removing sucrose in the swelling phase II (i.e. $\omega_{\mathrm{Sucrose}}^{\mathrm{EXT,II}} = 0$, $\omega_{\mathrm{Ions}}^{\mathrm{EXT,II}} = 1$). The duration of phases I and II is the same and is kept constant equal to 10 in non-dimensional time τ, i.e. about ten times longer than the characteristic time of water permeation. This choice is to ensure that the trans-membrane exchange of water and solutes may reach equilibrium as well as membrane relaxation may be completed within any single phase composing the osmotic cycle, at least in the base case of the parametric sweep analysis.

For the base case value of model parameters given in Table 4, the resulting temporal profiles of cell volume (ζ_{Cell}) with its water (ζ_{W}) and ion (ζ_{Ions}) contributions are reported in Figure 2 (top panels). Here the numerical solution of the SAR model (black lines) is compared with that of the two-parameter model (red lines) as obtained through the COMSOL Multiphysics® software run with a numerical tolerance of 10^{-6}. During phase I, cells shrink due to water exit and no difference in cell volume and its composition between the two models is shown, with a content of intracellular ions (ζ_{Ions}) remaining constant in time for both models. For the SAR model the temporal profiles of osmotic ($\Delta\omega$) and hydraulic pressure (Δp) gradients along with the ratio $\frac{\Phi_{\mathrm{Sph}}}{\Phi_{\mathrm{Ref}}}$ are also shown in Figure 2 (bottom panels). The osmotic driving force between the intra- and extra-cellular compartments ($\Delta\omega$) starts from a negative value and progressively increases as water exits the cell until vanishing at the end of phase I, when the osmotic equilibrium is reached. On the other hand, the hydraulic pressure counter-gradient (Δp) first decreases (starting from zero and becoming negative

counteracting water exit), then reverses the direction and starts increasing (remaining negative to keep on to counteract water exit), thus showing a minimum before vanishing at the end of phase I. This behaviour is due to membrane relaxation represented by the temporal profile of the ratio $\frac{\Phi_{\mathrm{Sph}}}{\Phi_{\mathrm{Ref}}}$ reported in Figure 2: an initial decrease of Φ_{Sph} triggered by water exosmosis with membrane tension becoming slack (see Equations 7-8), followed by a returning back to its resting condition as Φ_{Ref} catches up with Φ_{Sph} according to Equation 4 by removing excess membrane into membrane reservoirs. Accordingly, during the shrinking phase I MS channels remain closed and ions are not exchanged; the two-parameter and the SAR models show the same profiles for ζ_{Cell}, ζ_{W} and ζ_{Ions} and their simulations cannot be distinguished.

On the contrary, during phase II swelling occurs so that cell volume and water content increase as shown in Figure 2. Now, in the SAR model the cell membrane is stretched from the beginning of phase II but membrane relaxation is eventually completed once again as represented by the value of $\frac{\Phi_{\mathrm{Sph}}}{\Phi_{\mathrm{Ref}}}$: it promptly increases due to the increase of Φ_{Sph} triggered by osmosis, then reaches a maximum before returning back towards its initial value as Φ_{Ref} catches up with Φ_{Sph} through the recruitment of extra lipid bilayer from accessible membrane reservoirs. Accordingly, during the swelling phase II MS channels are always open and ions are exchanged in the SAR model, while they are impermeant in the two-parameter model. Now the simulations with the two models are different: since at the start of phase II the extracellular compartment is hypotonic with respect to cytoplasm (i.e. $\Delta\omega = \Delta\omega_{\mathrm{Ions}} > 0$), ion content inside the cell decreases in the SAR model. For this reason the amount of water entering the cells before equilibrium is eventually reached is lower with respect to the two-parameter model, and a cell volume smaller than the initial isotonic one is finally attained (i.e. $\zeta_{\mathrm{Cell}} = 0.859 \ @\ \tau = 20$).

A closer look to Figure 2 reveals that in the SAR model the hydrostatic pressure gradient $\Delta\mathrm{p}$ ($\sim 10^{-4}$) may be safely neglected with respect to $\Delta\omega$ (~ 1) when determining the driving force of water exchange rate represented by Equation 1. Together with the MS channels remaining closed these are the reasons why the temporal profiles of cell volume (ζ_{Cell}), water and ion content (ζ_{W} and ζ_{Ions}) from the SAR and the two-parameter models cannot be distinguished in phase I, while their difference in phase II may be ascribed only to ion exchange. Moreover by looking at the temporal profiles of $\frac{\Phi_{\mathrm{Sph}}}{\Phi_{\mathrm{Ref}}}$, membrane relaxation is the slowest phenomenon among those accounted for in the SAR model both in phase I and II, even though its constant is

about 100 times larger than water permeability (i.e. $\lambda_S \sim 10^2$ in Table 4). This behaviour is due to Φ_{Ref} which, regardless of the specific value assigned to λ_S, always follows water osmosis with some delay and tries to keep up with the variations of Φ_{Sph}, both slowing down when approaching the steady state.

The equilibrium conditions given by Equations 18-19 are plotted in Figure 3 for the base case (bold lines). Here, a perfect agreement is shown with the values (circles) reached by ζ_{Cell} at the end of phase I and II taken from the corresponding dynamic simulation of the SAR model reported in Figure 2 (i.e. $\zeta_{Cell}\ @\ \tau = 10$ and $\zeta_{Cell}\ @\ \tau = 20$ for phase I and II, respectively). Actually, as shown in Figure 3 this agreement may be extended to the cases when ion permeability is varied with respect to its base case value in the parametric sweep analysis, by using a smaller ($1.07 \cdot 10^{-3}$) and larger ($1.07 \cdot 10^{-2}$) λ_{Ions} (the corresponding dynamic simulations of the SAR model are reported in Figures S1-S2 in the supplementary material section, for the sake of brevity). The reason of this agreement is that the equilibrium equations were derived under the assumptions of a negligible hydrostatic pressure gradient and a relatively slow but complete membrane relaxation within every single phase of the osmotic cycle; as seen above, these are two conditions that result and are also met by dynamic simulations.

As clearly shown in Figure 3, only the swelling phase II is affected by the change of ion permeability, given that in the shrinking phase I membrane tension is slack, MS channels remain closed, and ions are not exchanged. More specifically, at the end of the osmotic cycle the recovery of the initial, isotonic cell volume in phase II is lower if λ_{Ions} increases, since a higher ion leakage from cells takes place during the swelling. Clearly when λ_{Ions} is equal to zero, the SAR model reduces to the two-parameter model and a perfect osmometer behaviour is obtained, with a complete recovery of the isotonic volume at the end of the osmotic cycle. On the other hand, when increasing ion permeability, the recovery of the isotonic cell volume achieved during phase II is progressively hindered, and the cells remain shrunk at the volume reached at the end of phase I.

To proceed with the parametric sweep analysis, the variation of the membrane relaxation rate constant λ_S is now investigated. The case of an infinitely slow membrane relaxation (i.e. $\lambda_S = 0$) for the SAR model is considered in Figure 4, where the temporal profiles of the same variables reported in Figure 2 are shown. Now Φ_{Ref} does not change with time and remain constant at its initial value according to Equation 4, while Φ_{Sph} follows the osmotic shrinkage and swelling during phase I and II, respectively. For this reason, in

Figure 4 the ratio $\frac{\Phi_{\mathrm{Sph}}}{\Phi_{\mathrm{Ref}}}$ is always smaller than its initial value, i.e. the cell membrane is always slack during the entire osmotic cycle and the initial resting condition is eventually reached only at the end of phase II. Thus, MS channels are always closed and no ion exchange takes place, i.e. a complete recovery of the isotonic cell volume is reached at the end of phase II ($\zeta_{\mathrm{Cell}} = 1 \ @ \ \tau = 20$), just like in the two-parameter model. Actually, in this case not only the final value at equilibrium but the full temporal profiles of cell volume (ζ_{Cell}) with its water (ζ_{W}) and ion (ζ_{Ions}) contributions simulated by the two models are the same during the whole osmotic cycle. However, this equivalence between the two models is only apparent and depends on the specific osmotic cycle investigated in this work: for instance, if the isotonic cells were contacted with a hypotonic instead of a hypertonic solution before returning to isotonic conditions (a simulation not shown for brevity), a stretched membrane with MS channels always open and the exchange of ions would be obtained in the SAR model even when $\lambda_{\mathrm{S}} = 0$. This would lead to an equilibrium cell volume at the end of the osmotic cycle different from the initial, isotonic one in the SAR model, while a complete recovery would be simulated by the two-parameter model as always. Therefore when an infinitely slow membrane relaxation is considered the SAR model does not reduce to the two-parameter model.

The case of $\lambda_{\mathrm{S}} = 8.42$ (i.e. about ten times smaller than its base case value) is reported in Figure 5 for the SAR model. In comparison with Figure 4, now ions are exchanged during phase II as it was for the base case shown in Figure 2: in particular, ion leakage starts when MS channels open since the membrane is stretched above its resting value, as highlighted by the vertical green line. However, the opening time of the MS channels does not coincide with the start of phase II as it was in Figure 2, but is delayed in time depending on λ_{S}: the lower λ_{S} the later the opening of MS channels with respect to the beginning of phase II. As a consequence, when gradually reducing the constant of membrane relaxation rate λ_{S}, a progressively shorter temporal window of MS channels opening during phase II is obtained so that no opening at all occurs when λ_{S} reaches its minimum value as shown in Figure 4. This narrowing down of the temporal window for MS channels opening in phase II as λ_{S} decreases causes a smaller ion leakage from the cells which in turn leads to a larger water swelling, and a more complete recovery of the isotonic cell volume at the end of the osmotic cycle (cf. Figure 2 with Figure 5 and then Figure 4, where $\zeta_{\mathrm{Cell}} \ @ \ \tau = 20$ changes from 0.859 to 0.908 and then 1, respectively).

Besides, in Figures 4-5 Δp ($\sim 10^{-3}$) is still negligible with respect to $\Delta\omega$ (~ 1) for the determination of the driving force of water exchange in Equation 1, whereas it is expected to increase much more when the membrane relaxation constant is reduced so significantly from the base case shown in Figure 2.

The low sensitivity of the SAR model to λ_S is highlighted in Figure 6, where the cell volume reached at the end of phase II when the dynamic simulation of the osmotic cycle is completed (i.e. $\zeta_{\mathrm{Cell}}\,@\,\tau = 20$) is reported in a semi-log plot to account for a wide variation of this parameter. It is shown that, starting from the base case (red symbol) an increase of 20 orders of magnitude for λ_S does not affect the cell volume attained at the end of phase II which remains constantly equal to 0.859, i.e. the same value given by the equilibrium condition plotted in Figure 3 for the base case. On the other hand, when λ_S is decreased from its base case value the final cell volume increases until reaching a complete recovery of the initial, isotonic cell volume. This is caused by a too slow membrane relaxation rate with respect to the other phenomena taken into account in the SAR model: in this region of the parametric space the relaxation of cell membrane is not completed within the shrinking phase I when lowering λ_S below a critical value and keeping constant the duration of the phase. Thus, when the swelling phase II starts membrane is still slack as in Figure 5, and MS channels do not open and ion leakage does not begin until enough water has entered the expanding cell and membrane stretching may begin. The determination of this precise moment is not easy unless by the numerical integration of the full set of ODEs and AEs in Tables 1-2, and the equilibrium conditions given by Equations 18-19 are not valid in this region of the parametric space. On the contrary, when membrane relaxation is relatively fast the equilibrium Equations 18-19 are capable to predict the system behaviour in a very wide range of λ_S as shown in Figure 6. Therefore, the validity of the derived equilibrium conditions may be extended not only to any value assigned to ion permeability λ_{Ions} but also to any value used for the constant of the membrane relaxation rate λ_S, provided that the phase duration is long enough that membrane relaxation is completed.

Besides, it is apparent that the two-parameter model represents the special subcase of the SAR model with an infinitely fast membrane relaxation, i.e. $\lambda_S = +\infty$. In fact, in such a limiting case Φ_{Ref} instantaneously follows the osmotic variations of Φ_{Sph}, so that the membrane is neither slack (in phase I) nor stretched (in phase II) but constantly kept at its resting tension, MS channels are always closed, and ions are never exchanged. Unfortunately, this cannot be shown through a numerical integration, since it is not possible to

set an infinite value for λ_S. Moreover, regardless of the specific numerical algorithm adopted to solve the equations of the model, a limitation on the use of very large numbers always emerges from the need to respect a numerical tolerance, depending on the accuracy of the computing machine.

A very similar behaviour shown by the SAR model when varying λ_S is obtained in the parametric sweep of the elastic modulus K' of cell membrane tension. For this reason, it is reported only in Figure S3 in the supplementary material section. In fact when reducing K' from its base case value a cell with a more elastic membrane is considered. This corresponds from one side to a reduced hydrostatic pressure difference Δp (becoming even more negligible with respect to the osmotic driving force $\Delta\omega$ in the water exchange rate), from the other to a slower membrane relaxation rate that is not completed within phase I. Therefore, when K' is gradually reduced the opening of MS channels during phase II is delayed and ion exchange begins progressively later than the start of phase II. Thus a reduced leakage of ions is obtained and the cell volume reached at the end of the osmotic cycle increases towards the complete recovery of the initial, isotonic cell volume. On the contrary, if K' increases above its base case value, membrane relaxation is fast enough to be concluded within phase I; now ion leakage starts at the very beginning of phase II, and cell volume at the end of any phase composing the osmotic cycle reaches the same values determined by the equilibrium conditions represented by Equations 18-19. Moreover, the hydrostatic pressure difference remains negligible in comparison with the osmotic driving force. Therefore, the validity of the equilibrium Equations 18-19 for the osmotic cycle with impermeant sucrose in the absence of a permeant CPA may be extended to any value assigned to the elastic modulus K', provided that the phase duration is long enough that cell membrane relaxation is completed. Besides, it is apparent that the SAR model reduces to the two-parameter model when considering an infinitely large elastic modulus, i.e. $K' = +\infty$. In this case, an infinitively rigid membrane that is kept always at resting condition is obtained. Again, this result cannot be shown through a numerical integration of model equations since an infinite value for K' cannot be set nor can very large numbers be used at a pre-set numerical tolerance.

Proceeding further with the parametric sweep analysis, a negligible sensitivity of the SAR model is found with respect to the resting tension Ω_R: wide variations of this parameter are capable to affect very slightly only the hydrostatic pressure difference Δp that remains negligible in comparison to $\Delta\omega$ anyway. For this reason, no further comments are reported in this work on this parameter, and the equilibrium conditions of

Equations 18-19 are always valid. On the contrary, the effect of β is shown in Figure 7 where the cell volume reached at the end of phase II when the dynamic simulation of the osmotic cycle is completed (i.e. $\zeta_{\mathrm{Cell}}\ @\ \tau = 20$) is reported in a semi-log plot to account for a wide variation of this parameter. It is shown that by decreasing β from its base case value (red symbol) the numerical solution of the SAR model does not change and remains equal to 0.859, i.e. the same value given by the equilibrium conditions plotted in Figure 3. On the contrary, when this parameter increases the cell volume at the end of phase II shows a minimum, i.e. it first decreases then grows up to its maximum possible value in this simulation that corresponds to a complete recovery of the initial, isotonic cell volume. To understand this behavior it is worth noting that β represents the ratio between membrane thickness and isotonic cell radius. As such it greatly affects the hydrostatic pressure difference $\Delta\mathrm{p}$ determined through the Laplace law expressed by Equation 6. This is shown in detail in Figure 8 where the results of the simulations with the SAR and the two-parameter models are compared for the case of a three orders of magnitude increase with respect to the base case value, i.e. $\beta = 1.32 \cdot 10^{2}$: during the shrinking phase I the exosmosis of water driven by the osmotic driving force $\Delta\omega$ ($\sim$1) is now visibly hindered by the counter-gradient of hydrostatic pressure $\Delta\mathrm{p}$ ($\sim$0.3), and a slower osmosis results (cf. Figures 2 and 8). Despite this a complete membrane relaxation is still achieved in phase I since the ratio $\frac{\Phi_{\mathrm{Sph}}}{\Phi_{\mathrm{Ref}}}$ returns to its initial value. Moreover, the SAR and the two-parameter models share the same extension of the shrinkage of cell volume and water content albeit following different dynamic paths, given that MS channels are closed and no ion-exchange takes place. On the contrary, during phase II the stretching of cell membrane begins immediately when the phase starts: MS channels promptly open and ion leakage may occur from the beginning of the phase. In comparison with the base case reported in Figure 2, due to the large counter-gradient of hydrostatic pressure $\Delta\mathrm{p}$ that significantly limits the swelling of water driven by the osmotic driving force $\Delta\omega$, a more pronounced ion leakage is now obtained in phase II (cf. $\zeta_{\mathrm{Ions}}\ @\ \tau = 20$). As a consequence, less water swells back during phase II and a smaller cell volume is eventually reached at the end of the osmotic cycle (i.e. $\zeta_{\mathrm{Cell}} = 0.762\ @\ \tau = 20$). If parameter β increases even further (i.e. $\beta = 1.32 \cdot 10^{4}$, five orders of magnitude larger than its base case value, see Figure S4 in the supplementary material) the duration of phase I is not long enough for a complete membrane relaxation due to a very high

counter-gradient of hydrostatic pressure Δp ($\sim$1.2): in this case osmosis and cell volume excursions are basically stopped during the entire osmotic cycle, and a limited ion leakage takes place in phase II.

Basically these results confirm that the validity of the equilibrium conditions represented by Equations 18-19 is strictly confined to a negligible counter-gradient of the hydrostatic pressure Δp with respect to the osmotic driving force $\Delta\omega$, as it was originally assumed during the derivation [5]. However, it is worth noting that values of $\beta \geq 1$ are not really possible, given that membrane thickness is always smaller than cell radius. Thus, when limiting the results of the parametric sweep analysis to realistic values assigned to the model parameters, the derived equilibrium Equations 18-19 can be considered generally valid, and the hydrostatic pressure difference may be safely neglected to determine the driving force of water exchange in Equation 1. This conclusion represents a relevant simplification of the SAR model for future use but it is also a very reassuring result, given that a negligible hydrostatic pressure difference across the membrane of any animal cell is a reiterated assumption in the literature of cryopreservation, physiology and bio-physics addressing the modelling of cell osmosis and the control of cell volume and shape.

Osmotic cycle with permeant DMSO in the absence of impermeant sucrose

The case of cells in contact with permeant DMSO in the absence of sucrose is examined to highlight the effect of CPA permeability λ_{CPA}. More specifically, the investigated osmotic cycle consists of isotonic cells first suspended in a hypertonic solution of DMSO added to isotonic ions (like PBS) in phase I ($\omega_{\mathrm{CPA}}^{\mathrm{EXT,I}} = 5.67$, $\omega_{\mathrm{Ions}}^{\mathrm{EXT,I}} = 1$), followed by CPA removal in phase II by returning back to isotonic ions ($\omega_{\mathrm{CPA}}^{\mathrm{EXT,II}} = 0$, $\omega_{\mathrm{Ions}}^{\mathrm{EXT,II}} = 1$). For the base case parameter values given in Table 4, the resulting temporal profiles of cell volume with its water, ion and CPA contributions are reported in Figure 9 (top panels) for the two-parameter and the SAR models.

During phase I DMSO is loaded into cell cytoplasm (ζ_{CPA}) and the well-known shrink-swell dynamics followed by the cell volume (ζ_{Cell}) is obtained with both models: isotonic cells suspended in a hypertonic solution initially shrink by losing water and accumulating CPA to increase internal osmolality, until the external osmolality is first reached and then overcome when cells start swelling back, thus showing a minimum in volume excursion. The two-parameter and SAR models show the same temporal profiles

exclusively up to a point indicated by the first green line shown in Figure 9, when stretching of cell membrane begins after the swelling has already started. At this point, MS channels open and ion leakage from the now hypertonic cells begins in the SAR model, while a constant ion content inside the cells is simulated by the two-parameter model. As a consequence, in the two-parameter model the cell volume reached at the end of phase I is larger than both its initial, isotonic value (due to CPA addition to cytoplasm) and the corresponding cell volume simulated by the SAR model, where a simultaneous ion leakage took place. Generally speaking, the cell volume reached at the end of phase I in the SAR model may result above, equal to, or below, the initial, isotonic cell volume: it depends on the extent of ion leakage during CPA addition which varies with the parameter values and operating conditions. In Figure 9, in particular, the cell volume reached at the end of phase I in the SAR model is lower than the initial, isotonic cell volume since a relatively extended ion leakage with respect to CPA addition is obtained with the adopted parameter values and operating conditions. As shown in the middle panel of Figure 9, the CPA quantity loaded into the cells at the end of phase I is larger in the two- parameter model than in the SAR model. Moreover, cell membrane relaxation in the SAR model is completed within the duration of phase I, and the hydrostatic pressure difference is always negligible with respect to the osmotic gradient, as shown in the bottom panels of Figure 9.

During phase II, when removing DMSO the well-known swell-shrink dynamics is simulated by the two models. The cells initially swell by accumulating water and releasing CPA to reduce the internal osmolality even if in the SAR model intracellular ions increase, driven by the negative $\Delta\omega_{Ions}$ in Equation 16 resulting from the water uptake. This process continues until the external osmolality is first reached and then overcome so that cells shrink back, thus showing a maximum in volume excursion. In contrast with phase I, now the temporal profiles simulated by the two models are different for the whole duration of phase II: in the SAR model cells start to accumulate ions at the beginning of phase II when the membrane is promptly stretched and MS channels open, while a constant ion content is obtained with the two-parameter model. The ion exchange simulated by the SAR model continues until membrane relaxation is eventually reached as indicated by the second vertical green line shown in Figure 9. The late opening of MS channels with respect to the start of phase I is responsible of the different extent of the ion exchange in the SAR model between the two phases composing the osmotic cycle: more ions enter the cells in phase II than exit in phase I as clearly

shown in Figure 9. As a consequence, at the end of the osmotic cycle the water content and cell volume are larger than their initial isotonic values in the SAR model (i.e. $\zeta_{\mathrm{Cell}} = 1.197 \,@\, \tau = 20$), while a complete recovery is obtained according to the two-parameter model.

The temporary opening of MS channels in the SAR model is represented by the temporal window contained between the two vertical green lines shown in Figure 9, whose position depends on the values of the model parameters as well as on the operating conditions (such as external osmolality and its composition, system temperature, and phase duration). Cell volume and its components reached at the end of the osmotic cycle depend on the position of this temporal window which cannot be determined easily for any possible run unless by a numerical integration of system dynamics represented by the entire set of ODEs and AEs of the SAR model. This is what prevents the derivation from the SAR model of the equilibrium conditions for the osmotic cycle with a permeant CPA. On the contrary, for the osmotic cycle with impermeant sucrose in the absence of CPA the position of this temporal window may be easily predicted: if phases I and II are sufficiently long, MS channels remain closed or open respectively, without any switching during the whole duration of any single phase, and the equilibrium conditions represented by Equations 18-19 in Table 3 can be derived.

To demonstrate the relevant role played by the position of the temporary opening of MS channels and the irregularities of the simulations with the SAR model, the osmotic cycle when the adopted CPA permeability λ_{CPA} is one order of magnitude smaller than its base case value is shown in Figure 10. As expected, the system response is generally slower for both the two-parameter and the SAR models when compared with the base case (cf. Figures 9 and 10). In particular, the shrink-swell dynamics of phase I is still simulated by both models with a more pronounced initial cell shrinkage before swelling starts, as expected. Accordingly the opening of MS channels in the SAR model is delayed with respect to the base case. Despite this, a larger ion leakage is obtained (cf. $\zeta_{\mathrm{Ions}} \,@\, \tau = 10$ in Figures 9 and 10). This unexpected behavior is due to a faster ion exchange as determined by Equation 3: when a lower λ_{CPA} is used an increased driving force $\Delta\omega_{\mathrm{Ions}}$ results from the more pronounced initial shrinkage of cell volume and water exosmosis. Regarding this aspect it is worth noting that when further decreasing λ_{CPA} to critical values the case of an impermeant CPA is eventually simulated: if phase duration is maintained constant, the shrink-swell dynamics of phase I progressively disappears being replaced by only shrinkage. In such a limiting case, since no opening of MS

channels occurs during phase I, the corresponding simulations with the SAR and the two-parameter models cannot be distinguished anymore for the whole phase I, and a constant ion content inside the cells is obtained with both models. Therefore, in the SAR model the extent of ion leakage during phase I shows a maximum when λ_{CPA} is reduced starting from the base case value while keeping constant the duration of the phase; this corresponds to a minimum in water and CPA content ($\zeta_{\mathrm{W}}, \zeta_{\mathrm{CPA}}$ @ $\tau = 10$) as well as in cell volume (ζ_{Cell} @ $\tau = 10$) lower than the initial, isotonic value. This is just an example of the complexity and irregularity of the system behaviour simulated by the SAR model in comparison with the two-parameter formalism. This irregularity of the SAR model outcomes is due to the non-linear interconnection among all the different phenomena accounted for, and increases significantly when varying the operating conditions (such as external osmolality and its composition, system temperature, and phase duration) instead of keeping them constant as in this work.

Another example of the irregularity in the SAR model outcomes is obtained in the phase II shown in Figure 10: when CPA permeability is decreased with respect to its base case value, the characteristic swell-shrink dynamics of phase II is still simulated by the two-parameter model whereas it is lost in the SAR model. According to the latter one, only swelling occurs and MS channels are never closed. As a consequence, while in the two-parameter model cells return back to the initial isotonic volume at the end of the osmotic cycle with a complete CPA removal and a constant ion content, in the SAR model cell volume levels up to a larger value, with CPA totally removed but with an increased content of intracellular ions in comparison with the initial, isotonic conditions. This peculiar osmotic response is due to a critically slow CPA removal rate: when λ_{CPA} is reduced, during phase II CPA inside the cells is retained more than in the base case; even if water swelling has already started the cells remain hypertonic with respect to the suspending solution, the cell membrane remains stretched and MS channels open so that the extracellular ions continue to enter the cells until membrane relaxation is eventually completed.

To conclude the parametric sweep analysis, when CPA permeability is increased one order of magnitude with respect to its base case value, the system response is generally faster for both models (cf. Figure S5 in supplementary material): as expected, in the SAR model the opening and closing of MS channels are anticipated in phase I and II, respectively, with preservation of shrink-swell dynamics followed by the swell-shrink one. It is worth noting that, the order of magnitude for the water and CPA exchange rates considered

in this case are comparable (i.e. $\lambda_{\mathrm{CPA}} = 6.26 \cdot 10^{-1}$), while ion exchange is much slower ($\lambda_{\mathrm{Ions}} = 2.14 \cdot 10^{-3}$ in Table 4). As a consequence, during phase I and II only water and CPA are actually exchanged, with ion content remaining nearly constant even in the SAR model, regardless of the opening of MS channels. Accordingly, a limited cell volume excursion is obtained, and a very similar system response is simulated by the two-parameter and SAR models: in other words, when CPA permeability increases towards water permeability the SAR model reduces to the two-parameter model due to a negligible ion exchange.

Concluding remarks

In this work, the recently proposed SAR model is addressed in contrast with the classic two-parameter model to describe the non-perfect osmotic behaviour of a cell suspension during cryopreservation. First, an appropriate non-dimensional version of the model equations is derived to identify the relevant non-dimensional parameters. Then, a parametric sweep analysis is performed and discussed to highlight the features of the proposed model. It is shown that the SAR model progressively reduces to the two-parameter formalism when a negligible ion/salt exchange between intra- and extra-cellular compartments takes place, i.e. when ion/salt permeability is reduced below a critical value or CPA permeability is increased above a critical one. For the same reason, the SAR model with a cell membrane characterized by zero elasticity or infinite constant of relaxation rate is equivalent to the two-parameter model, given that at these extreme conditions MS channels cannot open.

Generally speaking, in the SAR model cell volume and its composition at equilibrium are shown to depend on the position of the temporal window of MS channels opening, which is a complex function of model parameters and operating conditions: whereas at the end of any osmotic cycle a complete recovery of the initial, isotonic cell volume always results from the two-parameter model, in general a larger or lower cell volume is obtained with the new model, depending on the exact opening and closing time of MS channels during the osmotic excursions. This is not the case when the osmotic cycle with an impermeant solute like sucrose is used, where MS channels are open only during phase II when cells are suspended back in an isotonic solution. For this reason, with the SAR model only equilibrium equations after contact with impermeant sucrose may be analytically derived, albeit without the advantageous linearity of the Boyle

Van't Hoff equation. This paper demonstrates that the validity of these osmotic equilibrium equations with impermeant sucrose may be extended to any realistic set of model parameters, provided that enough time is allowed to the cell membrane for a complete relaxation. On the other hand, when a permeant CPA comes into play, a numerical integration of system dynamics, prolonged until steady state is eventually reached, is required to determine cell volume at equilibrium.

Finally, when determining the rate of water exchange a negligible hydrostatic pressure gradient across the cell membrane is obtained for any realistic set of the model parameter values. While representing a justification to simplify the dynamic version of the SAR model for future use, this confirms that animal cells are well-known to possess a very fragile membrane made only of a double layer of phospholipid molecules. Despite this simplification of the SAR model, this paper shows that the mechanics of the cell membrane coupled with surface area regulation may be considered responsible for ion/salt exchange and the control of cell volume during cryopreservation without resorting to the complex pump and leak physiological model.

Acknowledgements

This work was supported by the European Union's Horizon 2020 research and innovation programme [grant numbers 734434]. The funders had no role in study design, data collection and analysis, decision to publish, or preparation of the manuscript.

G.T. performed his activity in the framework of the International PhD in Innovation Sciences and Technologies at the Università degli Studi di Cagliari, Italy.

Appendix

The non-dimensionalization procedure used in this work starts from the set of dimensional equations of the SAR model reported in Tables A1 and A2 [5]. The name of the dimensional variables is defined with units in the notation section.

First, the non-dimensional variables need to be defined. This is obtained by scaling all the variables appearing in Tables A1 and A2 with a proper, constant value used as a reference indicated by *, i.e. (non-dim. var.) = (dim. var.) / (dim. var.*).

In particular, by taking advantage of the spherical shape of the cell, all the variables related to cell size (i.e. volume, surface, and radius) may be referred to a single, representative quantity which is the isotonic cell volume V^0_{Cell}. Thus, for the variables representing volume contributions to the cell, the chosen reference value (dim. var.*) is V^0_{Cell}, so that the non-dimensional variables are defined as $\zeta_{\mathrm{Cell}} = \frac{V_{\mathrm{Cell}}}{V^0_{\mathrm{Cell}}}$, $\zeta_{\mathrm{W}} = \frac{V_{\mathrm{W}}}{V^0_{\mathrm{Cell}}}$, $\zeta_{\mathrm{CPA}} = \frac{V_{\mathrm{CPA}}}{V^0_{\mathrm{Cell}}}$, and $\zeta_{\mathrm{Ions}} = \frac{V_{\mathrm{Ions}}}{V^0_{\mathrm{Cell}}}$.

Accordingly, for the variables representing the areas of membrane surface, the chosen reference value (dim. var.*) is the spherical area S^0_{Sph} corresponding to V^0_{Cell} (i.e. $S^0_{\mathrm{Sph}} = (4\pi)^{\frac{1}{3}} \left(3\, V^0_{\mathrm{Cell}}\right)^{\frac{2}{3}}$), so that the non-dimensional variables are defined as $\Phi_{\mathrm{Ref}} = \frac{S_{\mathrm{Ref}}}{S^0_{\mathrm{Sph}}}$ and $\Phi_{\mathrm{Sph}} = \frac{S_{\mathrm{Sph}}}{S^0_{\mathrm{Sph}}}$. Along these lines, the radius of the spherical cell may be determined from ζ_{Cell} as $r = \left(\frac{3\, V^0_{\mathrm{Cell}}\, \zeta_{\mathrm{Cell}}}{4\,\pi}\right)^{\frac{1}{3}}$.

For the variables representing osmolality, the chosen reference value (dim. var.*) is the isotonic osmolality M^0, both for the intra- as well as the extra-cellular compartments, so that the non-dimensional variables are defined as $\omega = \frac{\mathrm{M}}{\mathrm{M}^0}$, $\omega_{\mathrm{CPA}} = \frac{\mathrm{M}_{\mathrm{CPA}}}{\mathrm{M}^0}$, $\omega_{\mathrm{Ions}} = \frac{\mathrm{M}_{\mathrm{Ions}}}{\mathrm{M}^0}$, and $\omega_{\mathrm{Sucrose}} = \frac{\mathrm{M}_{\mathrm{Sucrose}}}{\mathrm{M}^0}$.

Accordingly, on the basis of the Van't Hoff Equation A.10 for the variables representing the hydrostatic pressure both for the intra- as well as the extra-cellular compartments, and membrane tension and its resting condition, the chosen reference value (dim. var.*) is $RT\,\mathrm{M}^0$ (with system temperature assumed constant during any simulation), so that the non-dimensional variables are defined as $\mathrm{p} = \frac{\mathrm{P}}{RT\,\mathrm{M}^0}$, $\Omega = \frac{\sigma}{RT\mathrm{M}^0}$, and $\Omega_{\mathrm{R}} = \frac{\sigma_{\mathrm{R}}}{RT\mathrm{M}^0}$, respectively.

Different from the previous non-dimensionalizations, for the non-dimensional time defined as $\tau = \frac{t}{t^*}$ the reference value t^* is left undetermined for now and will be defined only later.

By replacing the dimensional variables with the non-dimensional ones in Tables A1 and A2, the equation system of the SAR model in the pre-non-dimensional form reported in Tables A3 and A4 is obtained.

In particular, Equation A.18 is obtained by first combining Equations A.1 and A.10 to determine ΔΠ before replacing the dimensional variables with the non-dimensional ones. Analogously, the initial condition for Equation A.18 is obtained by first combining the initial conditions of Equations A.1 and A.3 to determine V_{Ions}^0 before replacing the dimensional variables with the non-dimensional ones.

From the pre-non-dimensional version, the final non-dimensional set of equations reported in Tables A5 and A6 may be derived. Now the time has come to determine the reference value t^* for variable t by setting equal to 1 the non-dimensional factor framed in Equation A.35, i.e. $t^* = \frac{V_{\mathrm{Cell}}^0}{L_{\mathrm{P}} S_{\mathrm{Sph}}^0 RT\mathrm{M}^0}$. The latter one is used in Equations A.36-A.38 for the definition of the non-dimensional CPA and Ion/salt permeability as well as membrane relaxation rate, namely λ_{CPA}, λ_{Ions}, and λ_{S}, respectively. This choice corresponds to scale all the kinetic parameters and time to water permeability L_{P}.

Table A1: ODEs of the SAR model in dimensional form [5].

Equation	Initial Condition	Number
$\frac{dV_{\mathrm{W}}}{dt} = -L_{\mathrm{P}} S_{\mathrm{Sph}} (\Delta \mathrm{P} - \Delta \Pi)$	$V_{\mathrm{W}}(0) = V_{\mathrm{W}}^{0} = \left(V_{\mathrm{Cell}}^{0} - V_{\mathrm{Ions}}^{0} - V_{\mathrm{B}} \right) \quad @ \quad t = 0$	(A.1)
$\frac{dV_{\mathrm{CPA}}}{dt} = -\tilde{v}_{\mathrm{CPA}} \, P_{\mathrm{CPA}} S_{\mathrm{Sph}} \Delta \mathrm{M}_{\mathrm{CPA}}$	$V_{\mathrm{CPA}}(0) = V_{\mathrm{CPA}}^{0} = 0 \quad @ \quad t = 0$	(A.2)
$\frac{dV_{\mathrm{Ions}}}{dt} = -P_{\mathrm{Ions}} S_{\mathrm{Sph}} \Delta \mathrm{M}_{\mathrm{Ions}}$	$V_{\mathrm{Ions}}(0) = V_{\mathrm{Ions}}^{0} = \frac{\left(V_{\mathrm{Cell}}^{0} - V_{\mathrm{B}} \right)}{1 + \frac{\varphi}{\tilde{v}_{\mathrm{Ions}} \mathrm{M}^{0}}} \quad @ \quad t = 0$	(A.3)
$\frac{dS_{\mathrm{Ref}}}{dt} = k_S \, S_{\mathrm{Ref}} \, \Delta \sigma$	$S_{\mathrm{Ref}}(0) = S_{\mathrm{Ref}}^{0} = \frac{S_{\mathrm{Sph}}^{0}}{1 + \frac{2\sigma_R}{K}} \quad @ \quad t = 0$	(A.4)

Table A2: AEs of the SAR model in dimensional form [5].

Equation	Number
$V_{\mathrm{Cell}} = V_{\mathrm{B}} + V_{\mathrm{Ions}} + V_{\mathrm{W}} + V_{\mathrm{CPA}}$	(A.5)
$\Delta \mathrm{P} = \mathrm{P}^{\mathrm{INT}} - \mathrm{P}^{\mathrm{EXT}} = \frac{2\,\mathrm{h}\,\Delta\sigma}{\mathrm{r}}$	(A.6)
$\Delta\sigma = \sigma - \sigma_{\mathrm{R}}$	(A.7)
$\sigma = \frac{K}{2}\left(\frac{S_{\mathrm{Sph}}}{S_{\mathrm{Ref}}} - 1\right)$	(A.8)
$S_{\mathrm{Sph}} = 4\pi\left(\frac{3V_{\mathrm{Cell}}}{4\pi}\right)^{\frac{2}{3}}$	(A.9)
$\Delta\Pi = RT\,\Delta\mathrm{M} = RT\left(\mathrm{M}^{\mathrm{INT}} - \mathrm{M}^{\mathrm{EXT}}\right)$	(A.10)
$\mathrm{M}^{\mathrm{INT}} = \mathrm{M}_{\mathrm{Ions}}^{\mathrm{INT}} + \mathrm{M}_{\mathrm{CPA}}^{\mathrm{INT}}$	(A.11)
$\mathrm{M}_{\mathrm{Ions}}^{\mathrm{INT}} = \frac{\varphi\, V_{\mathrm{Ions}}}{\tilde{v}_{\mathrm{Ions}}\, V_{\mathrm{W}}}$	(A.12)
$\mathrm{M}_{\mathrm{CPA}}^{\mathrm{INT}} = \frac{V_{\mathrm{CPA}}}{\tilde{v}_{\mathrm{CPA}}\, V_{\mathrm{W}}}$	(A.13)
$\mathrm{M}^{\mathrm{EXT}} = (\mathrm{M}_{\mathrm{Ions}}^{\mathrm{EXT}} + \mathrm{M}_{\mathrm{Sucrose}}^{\mathrm{EXT}} + \mathrm{M}_{\mathrm{CPA}}^{\mathrm{EXT}})$	(A.14)
$\Delta\mathrm{M}_{\mathrm{CPA}} = \mathrm{M}_{\mathrm{CPA}}^{\mathrm{INT}} - \mathrm{M}_{\mathrm{CPA}}^{\mathrm{EXT}}$	(A.15)
$\Delta\mathrm{M}_{\mathrm{Ions}} = \mathrm{M}_{\mathrm{Ions}}^{\mathrm{INT}} - \mathrm{M}_{\mathrm{Ions}}^{\mathrm{EXT}}$	(A.16)
$P_{\mathrm{Ions}} = \begin{cases} 0 & \Delta\sigma \le 0 \\ P_{\mathrm{Ions}} & \Delta\sigma > 0 \end{cases}$	(A.17)

Table A3: ODEs of the SAR model in pre-non-dimensional form.

Equation	Initial Condition	Number
$\frac{d\left(V_{\mathrm{Cell}}^{0}\,\zeta_{\mathrm{W}}\right)}{d(t^{*}\,\tau)} = -L_{\mathrm{P}}\left(S_{\mathrm{Sph}}^{0}\Phi_{\mathrm{Sph}}\right)(RT\mathrm{M}^{0}\Delta\mathrm{p} - RT\mathrm{M}^{0}\Delta\omega)$	$V_{\mathrm{Cell}}^{0}\,\zeta_{\mathrm{W}}(0) = V_{\mathrm{Cell}}^{0}\,\zeta_{\mathrm{W}}^{0} = V_{\mathrm{Cell}}^{0}\left(1 - \frac{1-\upsilon_{\mathrm{B}}}{1+\frac{\varphi}{\tilde{\upsilon}_{\mathrm{Ions}}\mathrm{M}^{0}}} - \upsilon_{\mathrm{B}}\right)$ @ $(t^{*}\,\tau) = 0$	(A.18)
$\frac{d\left(V_{\mathrm{Cell}}^{0}\,\zeta_{\mathrm{CPA}}\right)}{d(t^{*}\,\tau)} = -\tilde{\upsilon}_{\mathrm{CPA}}\,P_{\mathrm{CPA}}\left(S_{\mathrm{Sph}}^{0}\Phi_{\mathrm{Sph}}\right)(\mathrm{M}^{0}\,\Delta\omega_{\mathrm{CPA}})$	$V_{\mathrm{Cell}}^{0}\,\zeta_{\mathrm{CPA}}(0) = V_{\mathrm{Cell}}^{0}\,\zeta_{\mathrm{CPA}}^{0} = 0$ @ $(t^{*}\,\tau) = 0$	(A.19)
$\frac{d\left(V_{\mathrm{Cell}}^{0}\,\zeta_{\mathrm{Ions}}\right)}{d(t^{*}\,\tau)} = -P_{\mathrm{Ions}}\left(S_{\mathrm{Sph}}^{0}\Phi_{\mathrm{Sph}}\right)(\mathrm{M}^{0}\Delta\omega_{\mathrm{Ions}})$	$V_{\mathrm{Cell}}^{0}\,\zeta_{\mathrm{Ions}}(0) = V_{\mathrm{Cell}}^{0}\,\zeta_{\mathrm{Ions}}^{0} = V_{\mathrm{Cell}}^{0}\frac{(1-\upsilon_{\mathrm{B}})}{1+\frac{\varphi}{\tilde{\upsilon}_{\mathrm{Ions}}\mathrm{M}^{0}}}$ @ $(t^{*}\,\tau) = 0$	(A.20)
$\frac{d\left(S_{\mathrm{Sph}}^{0}\Phi_{\mathrm{Ref}}\right)}{d(t^{*}\,\tau)} = k_{S}\left(S_{\mathrm{Sph}}^{0}\Phi_{\mathrm{Ref}}\right)(RT\mathrm{M}^{0}\Delta\Omega)$	$S_{\mathrm{Sph}}^{0}\Phi_{\mathrm{Ref}}(0) = S_{\mathrm{Sph}}^{0}\Phi_{\mathrm{Ref}}^{0} = S_{\mathrm{Sph}}^{0}\frac{1}{1+2\frac{RT\,\mathrm{M}^{0}}{K}\frac{\sigma_{R}}{RT\,\mathrm{M}^{0}}}$ @ $(t^{*}\,\tau) = 0$	(A.21)

Table A4: AEs of the SAR model in pre-non-dimensional form.

Equation	Number
$V^0_{\mathrm{Cell}}\,\zeta_{\mathrm{Cell}} = V^0_{\mathrm{Cell}}\upsilon_{\mathrm{B}} + V^0_{\mathrm{Cell}}\,\zeta_{\mathrm{Ions}} + V^0_{\mathrm{Cell}}\,\zeta_{\mathrm{W}} + V^0_{\mathrm{Cell}}\,\zeta_{\mathrm{CPA}}$	(A.22)
$RT\mathrm{M}^0\Delta\mathrm{p} = RT\ \mathrm{M}^0\mathrm{p}^{\mathrm{INT}} - RT\ \mathrm{M}^0\mathrm{p}^{\mathrm{EXT}} = \dfrac{2\ \mathrm{h}\ RT\mathrm{M}^0\Delta\Omega}{\left(\dfrac{3\ V^0_{\mathrm{Cell}}\,\zeta_{\mathrm{Cell}}}{4\ \pi}\right)^{\frac{1}{3}}}$	(A.23)
$RT\mathrm{M}^0\Delta\Omega = \ RT\mathrm{M}^0\Omega - RT\mathrm{M}^0\Omega_{\mathrm{R}}$	(A.24)
$RT\mathrm{M}^0\Omega = \dfrac{K}{2}\left(\dfrac{S^0_{\mathrm{Sph}}\Phi_{\mathrm{Sph}}}{S^0_{\mathrm{Sph}}\Phi_{\mathrm{Ref}}} - 1\right)$	(A.25)
$S^0_{\mathrm{Sph}}\Phi_{\mathrm{Sph}} = 4\pi\left(\dfrac{3V^0_{\mathrm{Cell}}\,\zeta_{\mathrm{Cell}}}{4\pi}\right)^{\frac{2}{3}}$	(A.26)
$RT\mathrm{M}^0\Delta\omega = RT\left(\mathrm{M}^0\omega^{\mathrm{INT}} - \mathrm{M}^0\omega^{\mathrm{EXT}}\right)$	(A.27)
$\mathrm{M}^0\omega^{\mathrm{INT}} = \mathrm{M}^0\omega^{\mathrm{INT}}_{\mathrm{Ions}} + \mathrm{M}^0\omega^{\mathrm{INT}}_{\mathrm{CPA}}$	(A.28)
$\mathrm{M}^0\omega^{\mathrm{INT}}_{\mathrm{Ions}} = \dfrac{\varphi\ V^0_{\mathrm{Cell}}\,\zeta_{\mathrm{Ions}}}{\tilde{\upsilon}_{\mathrm{Ions}}\ V^0_{\mathrm{Cell}}\,\zeta_{\mathrm{W}}}$	(A.29)
$\mathrm{M}^0\omega^{\mathrm{INT}}_{\mathrm{CPA}} = \dfrac{V^0_{\mathrm{Cell}}\,\zeta_{\mathrm{CPA}}}{\tilde{\upsilon}_{\mathrm{CPA}}\ V^0_{\mathrm{Cell}}\,\zeta_{\mathrm{W}}}$	(A.30)
$\mathrm{M}^0\omega^{\mathrm{EXT}} = (\mathrm{M}^0\omega^{\mathrm{EXT}}_{\mathrm{Ions}} + \mathrm{M}^0\omega^{\mathrm{EXT}}_{\mathrm{Sucrose}} + \mathrm{M}^0\omega^{\mathrm{EXT}}_{\mathrm{CPA}})$	(A.31)
$\mathrm{M}^0\Delta\omega_{\mathrm{CPA}} = \mathrm{M}^0\omega^{\mathrm{INT}}_{\mathrm{CPA}} - \mathrm{M}^0\omega^{\mathrm{EXT}}_{\mathrm{CPA}}$	(A.32)
$\mathrm{M}^0\Delta\omega_{\mathrm{Ions}} = \mathrm{M}^0\omega^{\mathrm{INT}}_{\mathrm{Ions}} - \mathrm{M}^0\omega^{\mathrm{EXT}}_{\mathrm{Ions}}$	(A.33)
$P_{\mathrm{Ions}} = \begin{cases} 0 & RT\mathrm{M}^0\Delta\Omega \le 0 \\ P_{\mathrm{Ions}} & RT\mathrm{M}^0\Delta\Omega > 0 \end{cases}$	(A.34)

Table A5: ODEs of the SAR model in non-dimensional form.

Equation	Initial Condition	Number
$\frac{d\zeta_{\mathrm{W}}}{d\tau} = -\underbrace{\boxed{\left(\frac{t^*}{V_{\mathrm{Cell}}^0}\right) L_{\mathrm{P}} S_{\mathrm{Sph}}^0 RT\mathrm{M}^0}}_{=1} \Phi_{\mathrm{Sph}}(\Delta\mathrm{p} - \Delta\omega)$	$\zeta_{\mathrm{W}}(0) = \zeta_{\mathrm{W}}^0 = (1-\upsilon_{\mathrm{B}})\left(1 - \frac{1}{1+\underbrace{\boxed{\frac{\varphi}{\tilde{\upsilon}_{\mathrm{Ions}}\mathrm{M}^0}}}_{\frac{1}{\mu_{\mathrm{Ions}}}}}\right)$ @ $\tau = 0$	(A.35)
$\frac{d\zeta_{\mathrm{CPA}}}{d\tau} = -\underbrace{\boxed{\frac{\tilde{\upsilon}_{\mathrm{CPA}} P_{\mathrm{CPA}} \cancel{S_{\mathrm{Sph}}^0} \cancel{\mathrm{M}^0}}{L_{\mathrm{P}} \cancel{S_{\mathrm{Sph}}^0} RT \cancel{\mathrm{M}^0}}}}_{\lambda_{\mathrm{CPA}}} \Phi_{\mathrm{Sph}}\, \Delta\omega_{\mathrm{CPA}}$	$\zeta_{\mathrm{CPA}}(0) = \zeta_{\mathrm{CPA}}^0 = 0$ @ $\tau = 0$	(A.36)
$\frac{d\zeta_{\mathrm{Ions}}}{d\tau} = -\underbrace{\boxed{\frac{P_{\mathrm{Ions}}\, \cancel{S_{\mathrm{Sph}}^0} \cancel{\mathrm{M}^0}}{L_{\mathrm{P}} \cancel{S_{\mathrm{Sph}}^0} RT \cancel{\mathrm{M}^0}}}}_{\lambda_{\mathrm{Ions}}} \Phi_{\mathrm{Sph}} \Delta\omega_{\mathrm{Ions}}$	$\zeta_{\mathrm{Ions}}(0) = \zeta_{\mathrm{Ions}}^0 = \frac{(1-\upsilon_{\mathrm{B}})}{1+\underbrace{\boxed{\frac{\varphi}{\tilde{\upsilon}_{\mathrm{Ions}}\mathrm{M}^0}}}_{\frac{1}{\mu_{\mathrm{Ions}}}}}$ @ $\tau = 0$	(A.37)
$\frac{d\Phi_{\mathrm{Ref}}}{d\tau} = \underbrace{\boxed{\frac{k_S\ \cancel{S_{\mathrm{Sph}}^0}\ RT\ \cancel{\mathrm{M}^0}}{L_{\mathrm{P}} \cancel{S_{\mathrm{Sph}}^0} RT \cancel{\mathrm{M}^0}}\ \frac{V_{\mathrm{Cell}}^0}{S_{\mathrm{Sph}}^0}}}_{\lambda_{\mathrm{S}}} \Phi_{\mathrm{Ref}}\, \Delta\Omega$	$\Phi_{\mathrm{Ref}}(0) = \Phi_{\mathrm{Ref}}^0 = \frac{1}{1+\underbrace{\boxed{2\frac{RT\ \mathrm{M}^0}{K}}}_{\frac{1}{K'}}\underbrace{\boxed{\frac{\sigma_R}{RT\ \mathrm{M}^0}}}_{\Omega_{\mathrm{R}}}}$ @ $\tau = 0$	(A.38)

Table A6: AEs of the SAR model in non-dimensional form.

Equation	Number
$\zeta_{\mathrm{Cell}} = \upsilon_{\mathrm{B}} + \zeta_{\mathrm{Ions}} + \zeta_{\mathrm{W}} + \zeta_{\mathrm{CPA}}$	(A.39)
$\Delta \mathrm{p} = \mathrm{p}^{\mathrm{INT}} - \mathrm{p}^{\mathrm{EXT}} = \underbrace{\boxed{\frac{2\,\mathrm{h}}{\left(\frac{3\,V_{\mathrm{Cell}}^{0}}{4\,\pi}\right)^{\frac{1}{3}}}}}_{\beta} \frac{\Delta\Omega}{(\zeta_{\mathrm{Cell}})^{\frac{1}{3}}}$	(A.40)
$\Delta\Omega = \Omega - \Omega_{\mathrm{R}}$	(A.41)
$\Omega = \underbrace{\boxed{\frac{K}{2RT\mathrm{M}^{0}}}}_{K'} \left(\frac{\Phi_{\mathrm{Sph}}}{\Phi_{\mathrm{Ref}}} - 1\right)$	(A.42)
$\Phi_{\mathrm{Sph}} = \frac{4\pi}{S_{\mathrm{Sph}}^{0}} \left(\frac{3V_{\mathrm{Cell}}^{0}}{4\pi}\right)^{\frac{2}{3}} (\zeta_{\mathrm{Cell}})^{\frac{2}{3}}$	(A.43)
$\Delta\omega = \omega^{\mathrm{INT}} - \omega^{\mathrm{EXT}}$	(A.44)
$\omega^{\mathrm{INT}} = \omega_{\mathrm{Ions}}^{\mathrm{INT}} + \omega_{\mathrm{CPA}}^{\mathrm{INT}}$	(A.45)
$\omega_{\mathrm{Ions}}^{\mathrm{INT}} = \frac{\zeta_{\mathrm{Ions}}}{\underbrace{\boxed{\frac{\tilde{\upsilon}_{\mathrm{Ions}}\,\mathrm{M}^{0}}{\varphi}}}_{\mu_{\mathrm{Ions}}}} \zeta_{\mathrm{W}}$	(A.46)
$\omega_{\mathrm{CPA}}^{\mathrm{INT}} = \frac{\zeta_{\mathrm{CPA}}}{\underbrace{\boxed{\tilde{\upsilon}_{\mathrm{CPA}}\mathrm{M}^{0}}}_{\mu_{\mathrm{CPA}}}} \zeta_{\mathrm{W}}$	(A.47)
$\omega^{\mathrm{EXT}} = \omega_{\mathrm{Ions}}^{\mathrm{EXT}} + \omega_{\mathrm{Sucrose}}^{\mathrm{EXT}} + \omega_{\mathrm{CPA}}^{\mathrm{EXT}}$	(A.48)
$\Delta\omega_{\mathrm{CPA}} = \omega_{\mathrm{CPA}}^{\mathrm{INT}} - \omega_{\mathrm{CPA}}^{\mathrm{EXT}}$	(A.49)
$\Delta\omega_{\mathrm{Ions}} = \omega_{\mathrm{Ions}}^{\mathrm{INT}} - \omega_{\mathrm{Ions}}^{\mathrm{EXT}}$	(A.50)
$\underbrace{\boxed{\frac{P_{\mathrm{Ions}}}{L_{\mathrm{P}}\,R\,T}}}_{\lambda_{\mathrm{Ions}}} = \begin{cases} 0 & \Delta\Omega \leq 0 \\ \underbrace{\boxed{\frac{P_{\mathrm{Ions}}}{L_{\mathrm{P}}\,R\,T}}}_{\lambda_{\mathrm{Ions}}} & \Delta\Omega > 0 \end{cases}$	(A.51)

Notation

h	membrane thickness	[µm]
K	elastic modulus of the cell membrane	[Pa]
K'	non-dimensional elastic modulus of the cell membrane	[—]
k_{S}	constant of membrane relaxation rate	[Pa^{-1} s^{-1}]
L_{P}	water permeability	[µm Pa^{-1} s^{-1}]
M	osmolality	[mOsm L^{-1}]
p	non-dimensional hydrostatic pressure	[—]
P	hydrostatic pressure	[Pa]
P_{CPA}	CPA permeability	[µm s^{-1}]
P_{Ions}	ion permeability	[µm L s^{-1} $mOsm^{-1}$]
r	radius of the spherical cell	[µm]
R	universal gas constant	[J mol^{-1} K^{-1}]
S_{Ref}	membrane area of the cell used as reference to determine surface strain	[μm^2]
S_{Sph}	membrane area of the spherical cell	[μm^2]
t	time	[s]
T	absolute temperature	[K]
V_{B}	inactive volume	[μm^3]
V_{Cell}	cell volume	[μm^3]
V_{CPA}	intracellular CPA volume	[μm^3]
V_{Ions}	intracellular ion volume	[μm^3]
V_{W}	intracellular water volume	[μm^3]

Greek letters

β	non-dimensional cell membrane thickness	[—]
Δ	difference	[—]
ζ_{Cell}	non-dimensional cell volume	[—]
ζ_{CPA}	intracellular CPA volume fraction	[—]
ζ_{Ions}	intracellular ion volume fraction	[—]
ζ_{W}	intracellular water volume fraction	[—]
λ_{CPA}	ratio between CPA and water permeabilities	[—]
λ_{Ions}	ratio between ion and water permeabilities	[—]
λ_{S}	ratio between the constant of membrane relaxation rate and water permeability	[—]
μ_{CPA}	ratio between CPA and water intracellular volumes at isotonic conditions	[—]
μ_{Ions}	ratio between ion and water intracellular volumes at isotonic conditions	[—]

Π	osmotic pressure	[Pa]
σ	membrane tension	[Pa]
σ_R	membrane resting tension	[Pa]
τ	non-dimensional time	[—]
υ_B	inactive volume fraction	[—]
$\tilde{\upsilon}_{CPA}$	molar volume of CPA	[m^3 mol^{-1}]
$\tilde{\upsilon}_{Ions}$	molar volume of ions	[m^3 mol^{-1}]
Φ_{Ref}	non-dimensional membrane area of the cell used as reference to determine surface strain	[—]
Φ_{Sph}	non-dimensional membrane area of the spherical cell	[—]
φ	dissociation constant for ions/salt in water	[Osm mol^{-1}]
ω	non-dimensional osmolality	[—]
Ω	non-dimensional membrane tension	[—]
Ω_R	non-dimensional membrane resting tension	[—]

Superscript

0	initial or isotonic condition
I	phase I (addition of permeant or impermeant solute) of the osmotic cycle
II	phase II (removal of permeant or impermeant solute) of the osmotic cycle
INT	intracellular
EXT	extracellular
*	reference value for non-dimensional variable

References

[1] W.J. Armitage, Effect of solute concentration on intracellular water volume and hydraulic conductivity of human blood platelets, J. Physiol. 374 (1986) 375-385. https://doi.org/10.1113/jphysiol.1986.sp016085.

[2] A. Carlsen, J.O. Wieth, Glycerol transport in human red cells, Acta Physiol. Scand. 97 (1976) 501-513. https://doi.org/10.1111/j.1748-1716.1976.tb10290.x.

[3] E. Casula, G.P. Asuni, V. Sogos, A. Cincotti, hMSCs from UCB: isolation, characterization and determination of osmotic properties for optimal cryopreservation, Chem. Eng. Trans. 43 (2015) 265-270. https://doi.org/10.3303/CET1543045.

[4] E. Casula, G.P. Asuni, V. Sogos, S. Fadda, F. Delogu, A. Cincotti, Osmotic behaviour of human mesenchymal stem cells: implications for cryopreservation, Plos One 12 (2017) e0184180. https://doi.org/10.1371/journal.pone.0184180.

[5] E. Casula, G. Traversari, S. Fadda, O.V. Klymenko, C. Kontoravdi, A. Cincotti, Modelling the Osmotic Behaviour of Human Mesenchymal Stem Cells, Biochem. Eng. J. 151 (2019) e107296, https://doi.org/10.1016/j.bej.2019.107296.

[6] Z. Chen, K. Memon, Y. Cao, G. Zhao, A microfluidic approach for synchronous and nondestructive study of the permeability of multiple oocytes, Microsyst. Nanoeng. 6/55 (2020). https://doi.org/10.1038/s41378-020-0160-4.

[7] A. Cincotti, S. Fadda, Modeling the cryopreservation process of a suspension of cells: the effect of a size-distributed cell population, in L. Geris (Ed), Computational Modeling in Tissue Engineering, from series A. Gefen (Ed) Studies in Mechanobiology, Springer-Verlag Pub. Berlin Heidelberg, 2013, pp. 145-181. https://doi.org/10.1007/8415_2012_134.

[8] S. Fadda, A. Cincotti, G. Cao, A population balance approach for the description of water osmosis and intracellular ice formation during cryopreservation, Chemical Engineering Transactions 17 (2009) 1125-1130. https://doi.org/10.3303/CET0917188.

[9] S. Fadda, A. Cincotti, G. Cao, G., The effect of cell size distribution during the cooling stage of cryopreservation without CPA, AIChE J. 56 (2010) 2173-2185. https://doi.org/10.1002/aic.12137.

[10] S. Fadda, A. Cincotti, G. Cao, Rationalizing the equilibration and cooling stages of cryopreservation: the effect of cell size distribution, AIChE J. 57 (2011) 1075-1095. https://doi.org/10.1002/aic.12320.

[11] S. Fadda, H. Briesen, A. Cincotti, The effect of EIF dynamics on the cryopreservation process of a size distributed cell population, Cryobiology 62 (2011) 218-231. https://doi.org/10.1016/j.cryobiol.2011.03.006.

[12] J.A. Gilmore, L.E. Mcgann, J. Liu, D.Y. Gao, A.T. Peter, F.W. Kleinhans, J.K. Critser, Effect of cryoprotectant solutes on water permeability of human spermatozoa, Biol. Reproduction 53 (1995) 985-995. https://doi.org/10.1095/biolreprod53.5.985.

[13] X. Guo, Z. Chen, K. Memon, X. Chen, G. Zhao, An integrated microfluidic device for single cell trapping and osmotic behavior investigation of mouse oocytes, Cryobiology 92 (2020) 267-271. https://doi.org/10.1016/j.cryobiol.2019.09.016.

[14] E.K. Hoffmann, I.H. Lambert, S.F. Pedersen, Physiology of cell volume regulation in vertebrates, Physiol. Rev. 89 (2009) 193-277. https://doi.org/10.1152/physrev.00037.2007.

[15] H.Y. Jiang, S.X. Sun, Cellular pressure and volume regulation and implications for cell mechanics, Biophys. J. 105 (2013) 609-619. https://doi.org/10.1016/j.bpj.2013.06.021.

[16] J.O. Karlsson, M. Toner, M., Long-term storage of tissues by cryopreservation: critical issues, Biomaterials 17 (1996) 243-256. https://doi.org/10.1016/0142-9612(96)85562-1.

[17] J.O. Karlsson, M. Toner, Cryopreservation, in: R.P. Lanza, R. Langer, J. Vacanti (Eds), Principles of Tissue Engineering. 2nd Ed. Academic press, San Diego, 2000, pp. 293-307. https://doi.org/10.1007/11749219

[18] A.R. Kay, M.P. Blaustein, Evolution of our understanding of cell volume regulation by the pump-leak mechanism, J. Gen. Physiol. 51 (2019) 407-416, https://doi.org/10.1085/jgp.201812274.

[19] J. Keener, J., Sneyd, Mathematical Physiology I: Cellular Physiology, in S.S. Antman, J.E. Marsden, L. Sirovich (Eds), Interdisciplinary. Applied Mathematics series, Ed. Springer-Verlag, New York, 2009. https://doi.org/10.1007/978-0-387-79388-7.

[20] F.W. Kleinhans, Membrane permeability modeling: Kedem-Katchalsky vs a two-parameter formalism, Cryobiology 37 (1998) 271-289. https://doi.org/10.1006/cryo.1998.2135.

[21] F. Lang, G.L. Busch, M. Ritter, H. Völkl, S. Waldegger, E. Gulbins, D. Häussinger, D., Functional significance of cell volume regulatory mechanisms, Physiol. Rev. 78 (1998) 247-306. https://doi.org/10.1152/physrev.1998.78.1.247.

[22] J.M. Lahmann, J.D. Benson, A.Z. Higgins, Concentration dependence of the cell membrane permeability to cryoprotectant and water and implications for design of methods for post-thaw washing of human erythrocytes, Cryobiology 80 (2018) 1-11. https://doi.org/10.1016/j.cryobiol.2017.12.003.

[23] J.M. Lahmann, C. CruzSanchez, J.D. Benson, J.P. Acker, A.Z. Higgins, Implications of variability in cell membrane permeability for design of methods to remove glycerol from frozen-thawed erythrocytes, Cryobiology 92 (2020) 168-179. https://doi.org/10.1016/j.cryobiol.2020.01.006.

[24] P. Mazur, S.P. Leibo, E.H.Y. Chu, A two-factor hypothesis of freezing injury: evidence from chinese hamster tissue-culture cells, Exp. Cell Res. 71 (1972) 345-355. https://doi.org/10.1016/0014-4827(72)90303-5.

[25] R.C. Prickett, J.A.W. Elliott, S. Hakda, L.E. McGann, A non-ideal replacement for the Boyle van't Hoff equation, Cryobiology 57 (2008) 130-136. https://doi.org/10.1016/j.cryobiol.2008.07.002.

[26] L.U. Ross-Rodriguez, J.A.W: Elliott, L.E: McGann, Non-ideal solution thermodynamics of cytoplasm, Biopreserv. Biobank. 10 (2012) 462-471. https://doi.org/10.1089/bio.2012.0027.

[27] F. Sachs, M.V. Sivaselvan, Cell volume control in three dimensions: water movement without solute movement, J. Gen. Physiol. 145 (2015) 373-380. https://doi.org/10.1085/jgp.201411297.

[28] W.D. Stein, J.F. Danielli, Structure and function in red cell permeability, Discuss. Faraday Soc. 21 (1956) 238-251. https://doi.org/10.1039/DF9562100238.

[29] W.D. Stein, Spontaneous and enzyme-induced dimer formation and its role in membrane permeability. II. The mechanism of movement of glycerol across the human erythrocyte membrane, Biochim. Biophys. Acta 59 (1962) 47-65. https://doi.org/10.1016/0006-3002(62)90697-2.

[30] J. Tao, S.X. Sun, Active biochemical regulation of cell volume and a simple model of cell tension response, Biophys. J. 109 (2015) 1541-1550. https://doi.org/10.1016/j.bpj.2015.08.025.

[31] M.R. Toon, A.K. Solomon, Transport parameters in the human red cell membrane: solute-membrane interactions of hydrophilic alcohols and their effect on permeation, Biochim. Biophys. Acta 1022 (1990) 57-71. https://doi.org/10.1016/0005-2736(90)90400-I.

[32] W.F. Wolkers, H. Oldenhof, F. Tang, J. Han, J. Bigalk, H. Sieme, Factors Affecting the Membrane Permeability Barrier Function of Cells during Preservation Technologies, Langmuir 35 (2019) 7520-7528. https://doi.org/10.1021/acs.langmuir.8b02852.

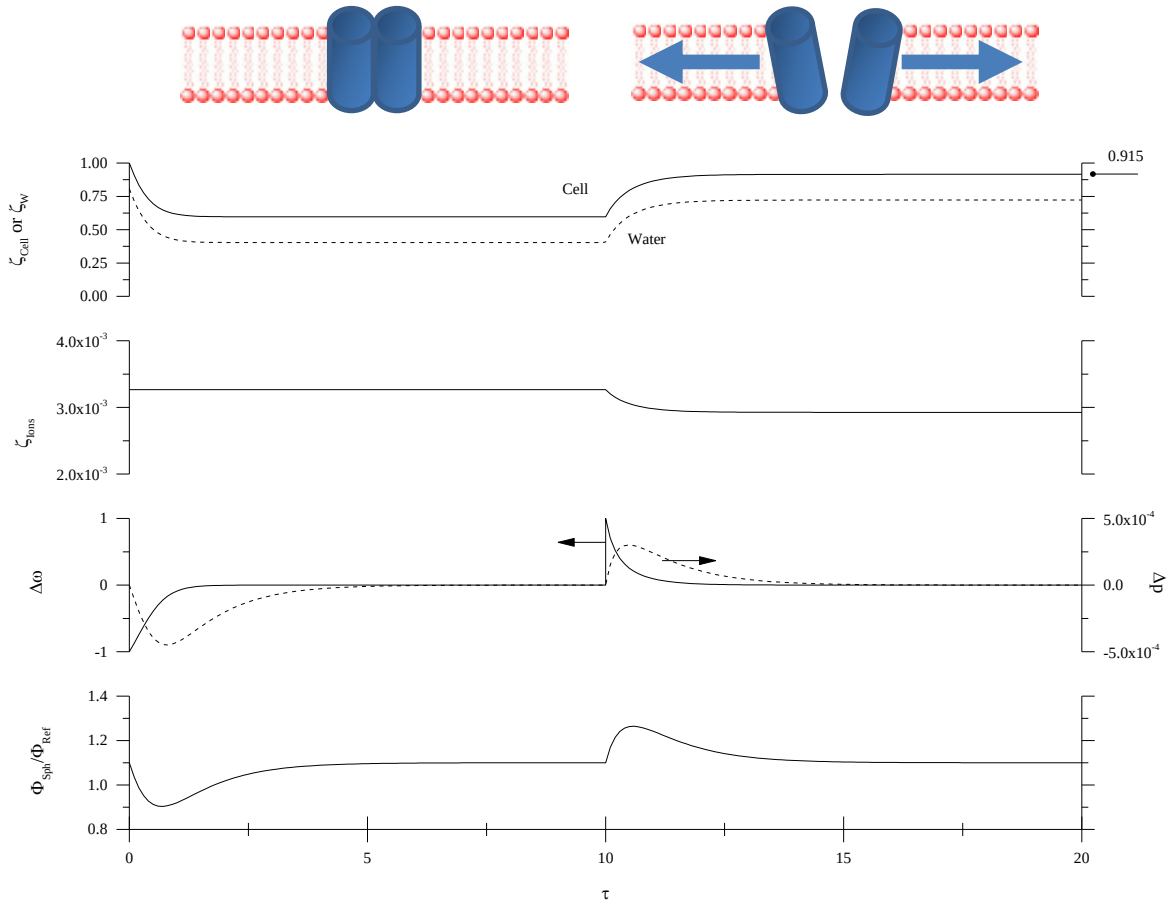

Figure S1: Osmotic cycle with impermeant sucrose in the absence of permeant CPA: results of the SAR model in the parameter sweep analysis when decreasing ion permeability ($\lambda_{\mathrm{Ions}} = 1.07 \cdot 10^{-3}$). The simulation of the two-parameter model is not reported because it does not change from Figure 2.

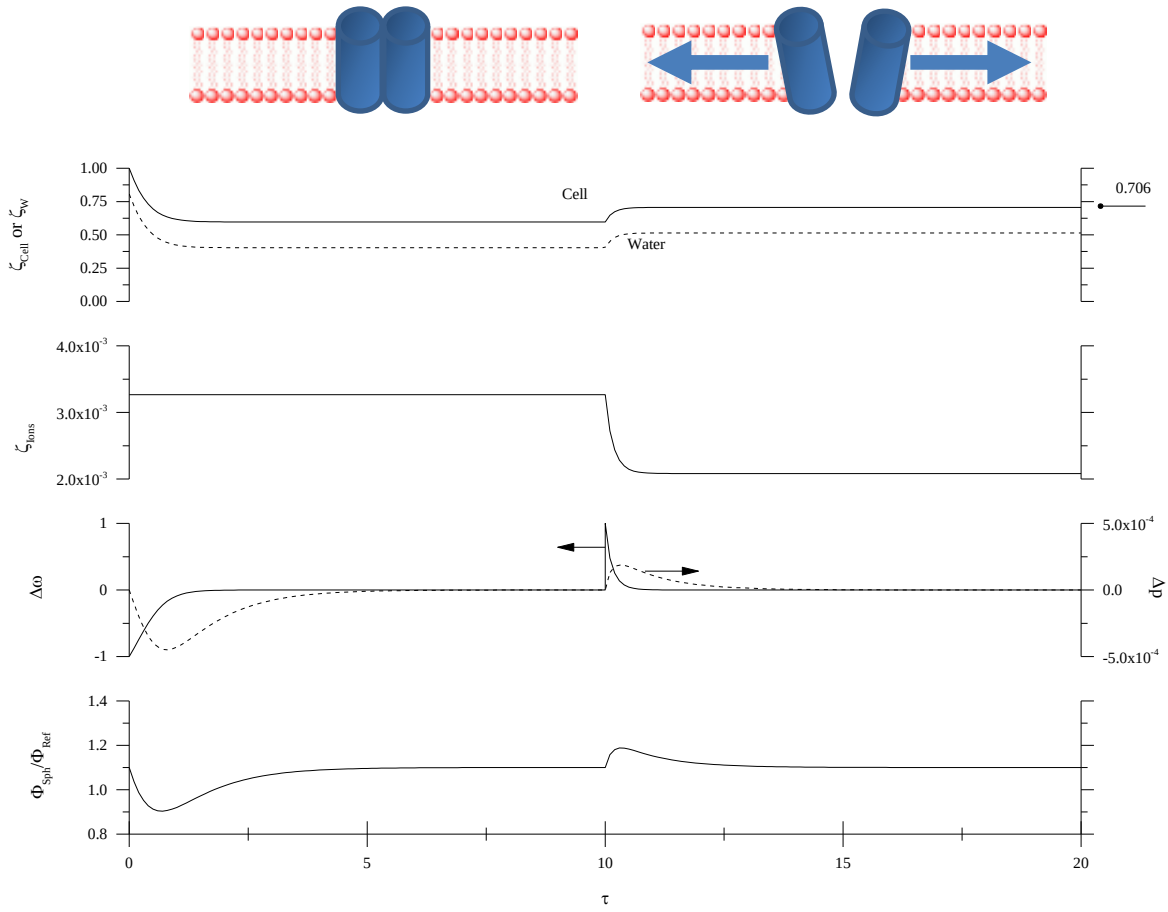

Figure S2: Osmotic cycle with impermeant sucrose in the absence of permeant CPA: results of the SAR model in the parameter sweep analysis when increasing ion permeability ($\lambda_{\mathrm{Ions}} = 1.07 \cdot 10^{-2}$). The simulation of the two-parameter model is not reported because it does not change from Figure 2.

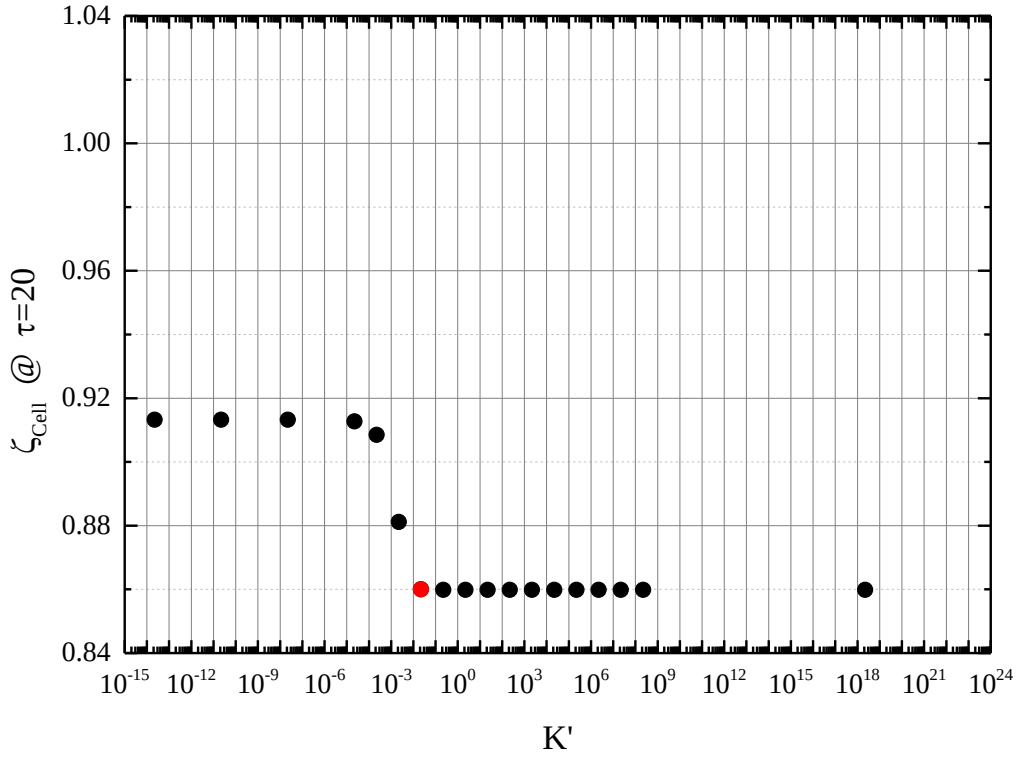

Figure S3: Osmotic cycle with impermeant sucrose in the absence of permeant CPA: results of the SAR model in terms of the cell volume at the end of phase II ($\zeta_{\mathrm{Cell}}\,@\,\tau = 20$) for the parameter sweep of K' (total duration of osmotic cycle is 20, i.e. 10 for both phase I and II); base case in red.

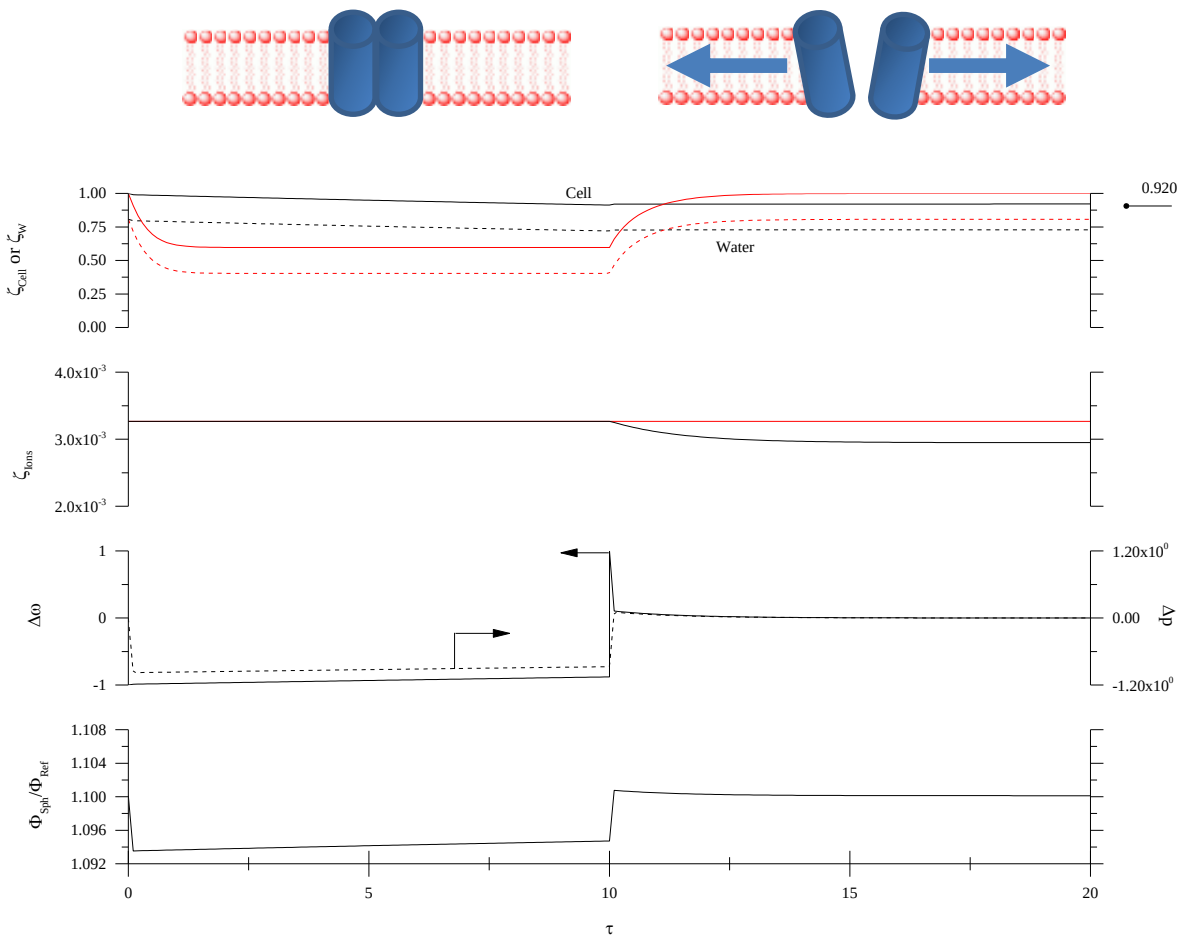

Figure S4: Osmotic cycle with impermeant sucrose in the absence of permeant CPA: comparisons between the results of the SAR model (black) and the two-parameter model (red) in the parameter sweep analysis with $\beta = 1.32 \cdot 10^4$, five orders of magnitude increase with respect to its base case value The simulation of the two-parameter model is reported even though it does not change with respect to Figure 2.

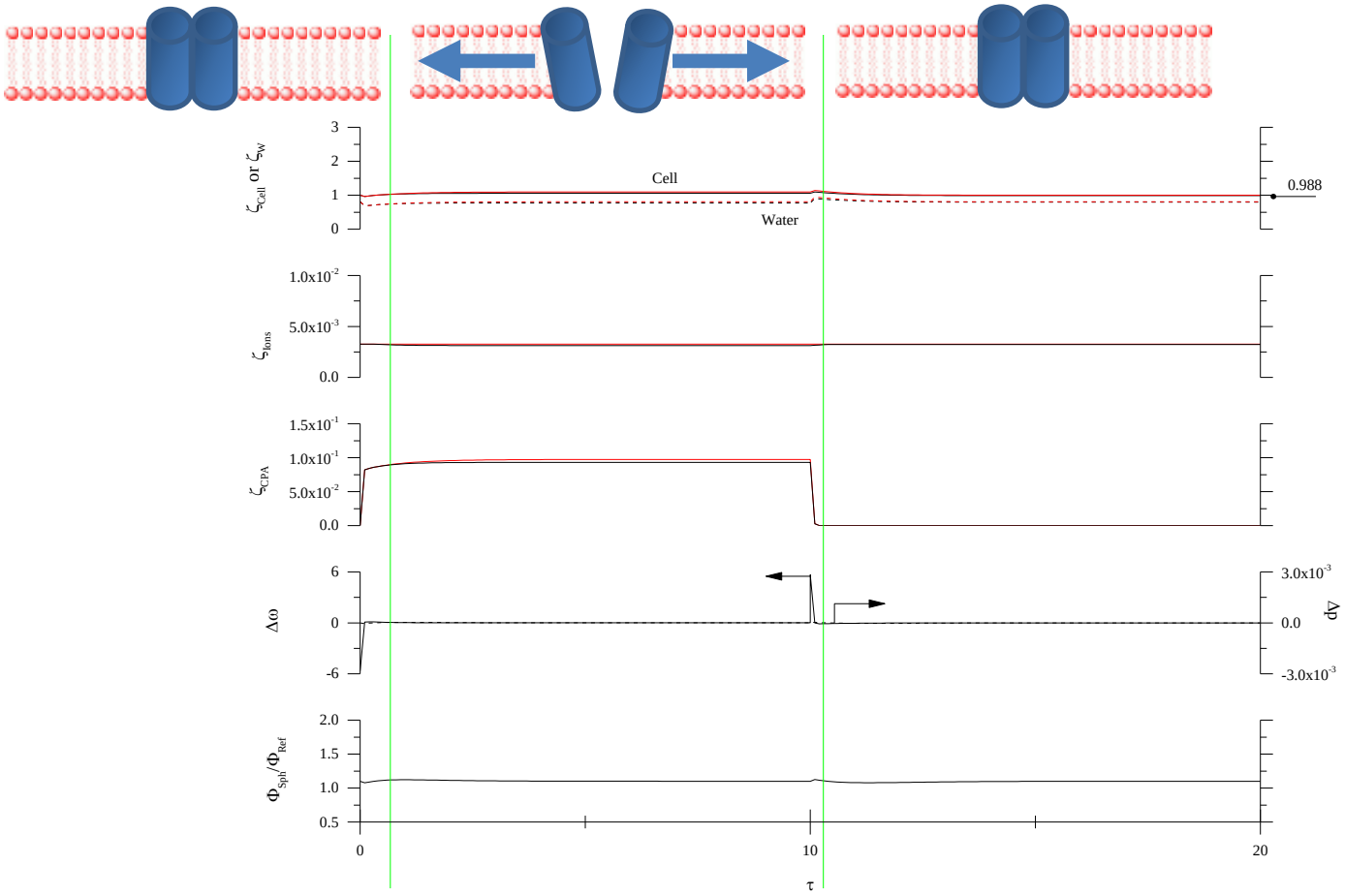

Figure S5: Osmotic cycle with permeant DMSO in the absence of impermeant sucrose: comparisons between the results of the SAR model (black) and the two-parameter model (red) in parameter sweep analysis with $\lambda_{CPA} = 6.26 \cdot 10^{-1}$, one order of magnitude increase with respect to its base case value. The vertical, green lines indicate opening and closing of MS channels.

Table 1: Ordinary Differential Equations (OEDs) of the SAR model in non-dimensional form.

Equation	Initial Condition	Number
$\frac{d\zeta_{\mathrm{W}}}{d\tau} = -\Phi_{\mathrm{Sph}}(\Delta \mathrm{p} - \Delta\omega)$	$\zeta_{\mathrm{W}}(0) = \zeta_{\mathrm{W}}^{0} = \left(\frac{1-\upsilon_{\mathrm{B}}}{1+\mu_{\mathrm{Ions}}}\right) \quad @ \quad \tau = 0$	(1)
$\frac{d\zeta_{\mathrm{CPA}}}{d\tau} = -\lambda_{\mathrm{CPA}}\, \Phi_{\mathrm{Sph}}\, \Delta\omega_{\mathrm{CPA}}$	$\zeta_{\mathrm{CPA}}(0) = \zeta_{\mathrm{CPA}}^{0} = 0 \quad @ \quad \tau = 0$	(2)
$\frac{d\zeta_{\mathrm{Ions}}}{d\tau} = -\lambda_{\mathrm{Ions}}\, \Phi_{\mathrm{Sph}}\, \Delta\omega_{\mathrm{Ions}}$	$\zeta_{\mathrm{Ions}}(0) = \zeta_{\mathrm{Ions}}^{0} = \mu_{\mathrm{Ions}}\left(\frac{1-\upsilon_{\mathrm{B}}}{1+\mu_{\mathrm{Ions}}}\right) \quad @ \quad \tau = 0$	(3)
$\frac{d\Phi_{\mathrm{Ref}}}{d\tau} = \lambda_{\mathrm{S}}\, \Phi_{\mathrm{Ref}}\, \Delta\Omega$	$\Phi_{\mathrm{Ref}}(0) = \Phi_{\mathrm{Ref}}^{0} = \left(\frac{1}{1+\frac{\Omega_{\mathrm{R}}}{K'}}\right) \quad @ \quad \tau = 0$	(4)

Table 2: Auxiliary Algebraic Equations (AEs) of the SAR model in non-dimensional form.

Equation	Number
$\zeta_{\mathrm{Cell}} = \upsilon_{\mathrm{B}} + \zeta_{\mathrm{Ions}} + \zeta_{\mathrm{W}} + \zeta_{\mathrm{CPA}}$	(5)
$\Delta \mathrm{p} = \mathrm{p}^{\mathrm{INT}} - \mathrm{p}^{\mathrm{EXT}} = \frac{\beta\, \Delta\Omega}{(\zeta_{\mathrm{Cell}})^{\frac{1}{3}}}$	(6)
$\Delta\Omega = \Omega - \Omega_{\mathrm{R}}$	(7)
$\Omega = K' \left(\frac{\Phi_{\mathrm{Sph}}}{\Phi_{\mathrm{Ref}}} - 1\right)$	(8)
$\Phi_{\mathrm{Sph}} = (\zeta_{\mathrm{Cell}})^{\frac{2}{3}}$	(9)
$\Delta\omega = \omega^{\mathrm{INT}} - \omega^{\mathrm{EXT}}$	(10)
$\omega^{\mathrm{INT}} = \omega_{\mathrm{Ions}}^{\mathrm{INT}} + \omega_{\mathrm{CPA}}^{\mathrm{INT}}$	(11)
$\omega_{\mathrm{Ions}}^{\mathrm{INT}} = \frac{\zeta_{\mathrm{Ions}}}{\mu_{\mathrm{Ions}}\, \zeta_{\mathrm{W}}}$	(12)
$\omega_{\mathrm{CPA}}^{\mathrm{INT}} = \frac{\zeta_{\mathrm{CPA}}}{\mu_{\mathrm{CPA}}\, \zeta_{\mathrm{W}}}$	(13)
$\omega^{\mathrm{EXT}} = (\omega_{\mathrm{Ions}}^{\mathrm{EXT}} + \omega_{\mathrm{Sucrose}}^{\mathrm{EXT}} + \omega_{\mathrm{CPA}}^{\mathrm{EXT}})$	(14)
$\Delta\omega_{\mathrm{CPA}} = \omega_{\mathrm{CPA}}^{\mathrm{INT}} - \omega_{\mathrm{CPA}}^{\mathrm{EXT}}$	(15)
$\Delta\omega_{\mathrm{Ions}} = \omega_{\mathrm{Ions}}^{\mathrm{INT}} - \omega_{\mathrm{Ions}}^{\mathrm{EXT}}$	(16)
$\lambda_{\mathrm{Ions}} = \begin{cases} 0 & \Delta\Omega \leq 0 \\ \lambda_{\mathrm{Ions}} & \Delta\Omega > 0 \end{cases}$	(17)

Table 3: Equilibrium conditions of the SAR model in non-dimensional form after an osmotic cycle with impermeant sucrose in the absence of CPA with $\omega^{\mathrm{EXT,\,II}} \leq \omega^{\mathrm{EXT,\,I}}$: phase I, contact with hypertonic solutions of sucrose and ions ($\omega^{\mathrm{EXT,\,I}} = \omega^{\mathrm{EXT,\,I}}_{\mathrm{Sucrose}} + \omega^{\mathrm{EXT,\,I}}_{\mathrm{Ions}}$); phase II, removing sucrose ($\omega^{\mathrm{EXT,\,II}} = \omega^{\mathrm{EXT,\,II}}_{\mathrm{Ions}}$).

Equation	Number
$\zeta^{\mathrm{I}}_{\mathrm{Cell}} = \underbrace{\upsilon_{\mathrm{B}}}_{\mathrm{Inactive}} + \underbrace{\left(\frac{1-\upsilon_{\mathrm{B}}}{1+\mu_{\mathrm{Ions}}}\right)\left(\frac{1}{\omega^{\mathrm{EXT,\,I}}}\right)}_{\mathrm{Water}} + \underbrace{\mu_{\mathrm{Ions}}\left(\frac{1-\upsilon_{\mathrm{B}}}{1+\mu_{\mathrm{Ions}}}\right)}_{\mathrm{Ions}}$	(18)
$\zeta^{\mathrm{II}}_{\mathrm{Cell}} = \underbrace{\upsilon_{\mathrm{B}}}_{\mathrm{Inactive}} + \underbrace{\left(\frac{1-\upsilon_{\mathrm{B}}}{1+\mu_{\mathrm{Ions}}}\right)\left(\frac{1}{\omega^{\mathrm{EXT,\,II}}}\right)\left(\frac{\mu_{\mathrm{Ions}}+\frac{\lambda_{\mathrm{Ions}}}{\omega^{\mathrm{EXT,\,I}}}}{\mu_{\mathrm{Ions}}+\frac{\lambda_{\mathrm{Ions}}}{\omega^{\mathrm{EXT,\,II}}}}\right)}_{\mathrm{Water}} + \underbrace{\mu_{\mathrm{Ions}}\left(\frac{1-\upsilon_{\mathrm{B}}}{1+\mu_{\mathrm{Ions}}}\right)\left(\frac{\mu_{\mathrm{Ions}}+\frac{\lambda_{\mathrm{Ions}}}{\omega^{\mathrm{EXT,\,I}}}}{\mu_{\mathrm{Ions}}+\frac{\lambda_{\mathrm{Ions}}}{\omega^{\mathrm{EXT,\,II}}}}\right)}_{\mathrm{Ions}}$	(19)

Table 4: Model parameters in non-dimensional form (base case) determined at a system temperature of 298 K, based on the parameter values reported in [5].

Parameter	**Expression**	**Value**
β	$\frac{2\,h}{\left(\frac{3}{4\pi}V_{\mathrm{Cell}}^{0}\right)^{\frac{1}{3}}}$	$1.32\cdot10^{-1}$
λ_{CPA}	$\frac{\tilde{v}_{\mathrm{CPA}}\,P_{\mathrm{CPA}}(T)}{L_{\mathrm{P}}(T)\,R\,T}$	$6.26\cdot10^{-2}$
λ_{Ions}	$\frac{P_{\mathrm{Ions}}(T)}{L_{\mathrm{P}}(T)\,R\,T}$	$2.14\cdot10^{-3}$
λ_{S}	$\frac{k_{\mathrm{S}}\left(\frac{3}{4\pi}V_{\mathrm{Cell}}^{0}\right)^{\frac{1}{3}}}{3\,L_{\mathrm{P}}(T)}$	$8.42\cdot10^{1}$
μ_{CPA}	$\tilde{v}_{\mathrm{CPA}}\,\mathrm{M}^{0}$	$2.13\cdot10^{-2}$
μ_{Ions}	$\frac{\tilde{v}_{\mathrm{Ions}}\,\mathrm{M}^{0}}{\varphi}$	$4.05\cdot10^{-3}$
K'	$\frac{K}{2\,R\,T\,\mathrm{M}^{0}}$	$2.22\cdot10^{-2}$
υ_{B}	$\frac{V_{\mathrm{B}}}{V_{\mathrm{Cell}}^{0}}$	0.2
Ω_{R}	$\frac{\sigma_{\mathrm{R}}}{R\,T\,\mathrm{M}^{0}}$	$1.11\cdot10^{-3}$

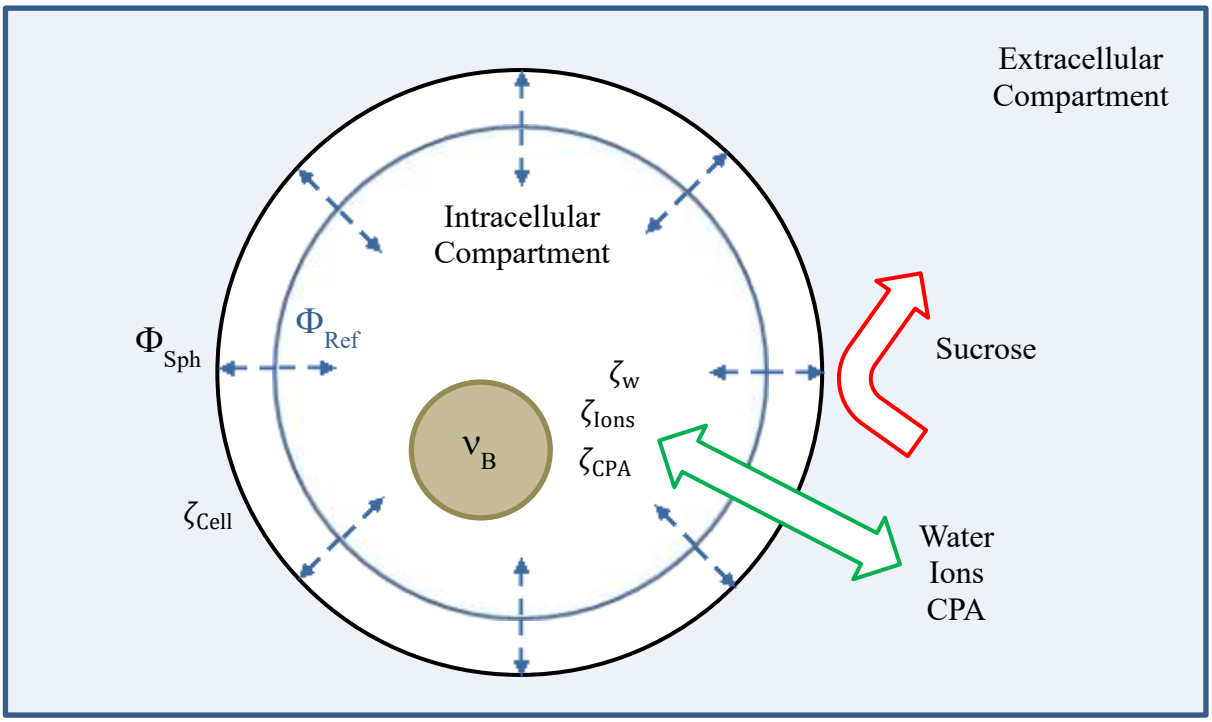

Figure 1: Schematic representation of a cell according to the SAR model.

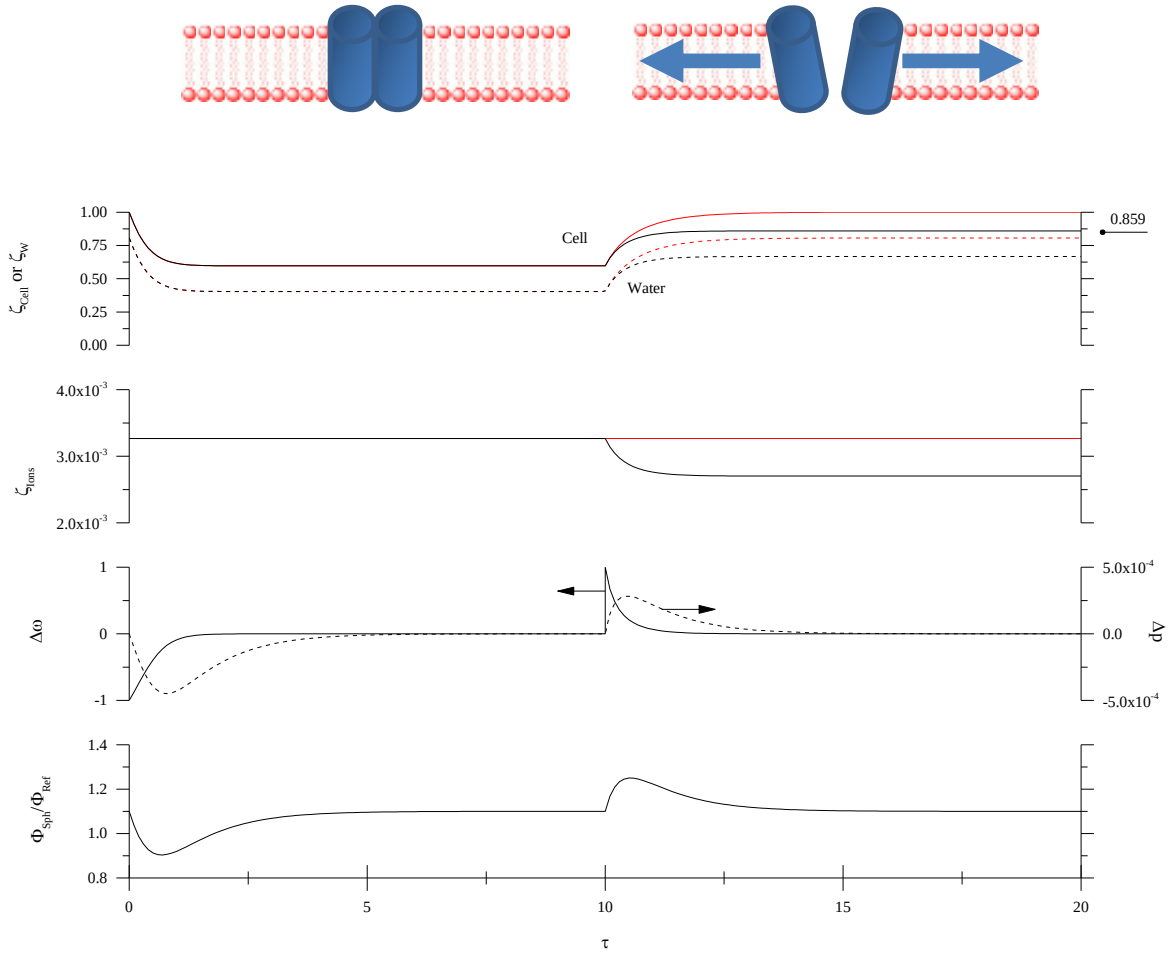

Figure 2: Osmotic cycle with impermeant sucrose in the absence of permeant CPA: comparisons between the results of the SAR model (black) and the two-parameter model (red) using the parameter values reported in Table 4 (base case).

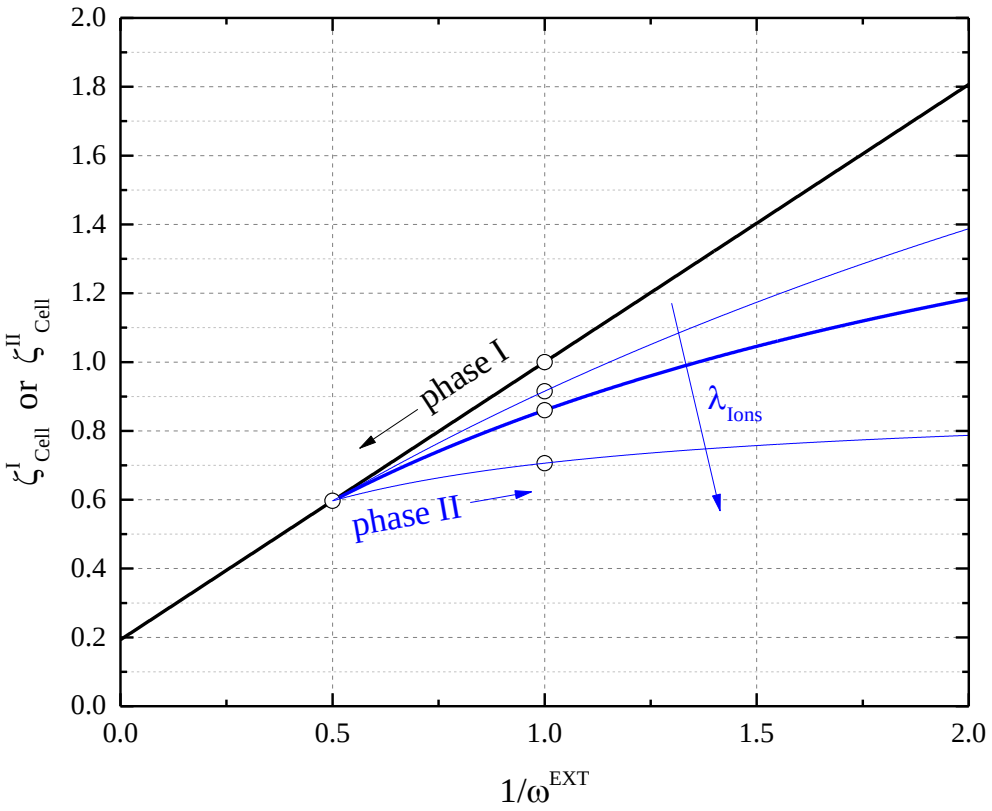

Figure 3: Equilibrium conditions ($\zeta^{\mathrm{I}}_{\mathrm{Cell}}$ and $\zeta^{\mathrm{II}}_{\mathrm{Cell}}$) of the SAR model for the osmotic cycle with sucrose in the parametric sweep analysis: variation of ion permeability ($\lambda_{\mathrm{Ions}} = 1.07 \cdot 10^{-3},\ 2.14 \cdot 10^{-3},\ 1.07 \cdot 10^{-2}$), with base case in bold lines. Circles represent the corresponding numerical integration of the dynamic SAR model (ζ_{Cell} @ $\tau = 10$ and ζ_{Cell} @ $\tau = 20$).

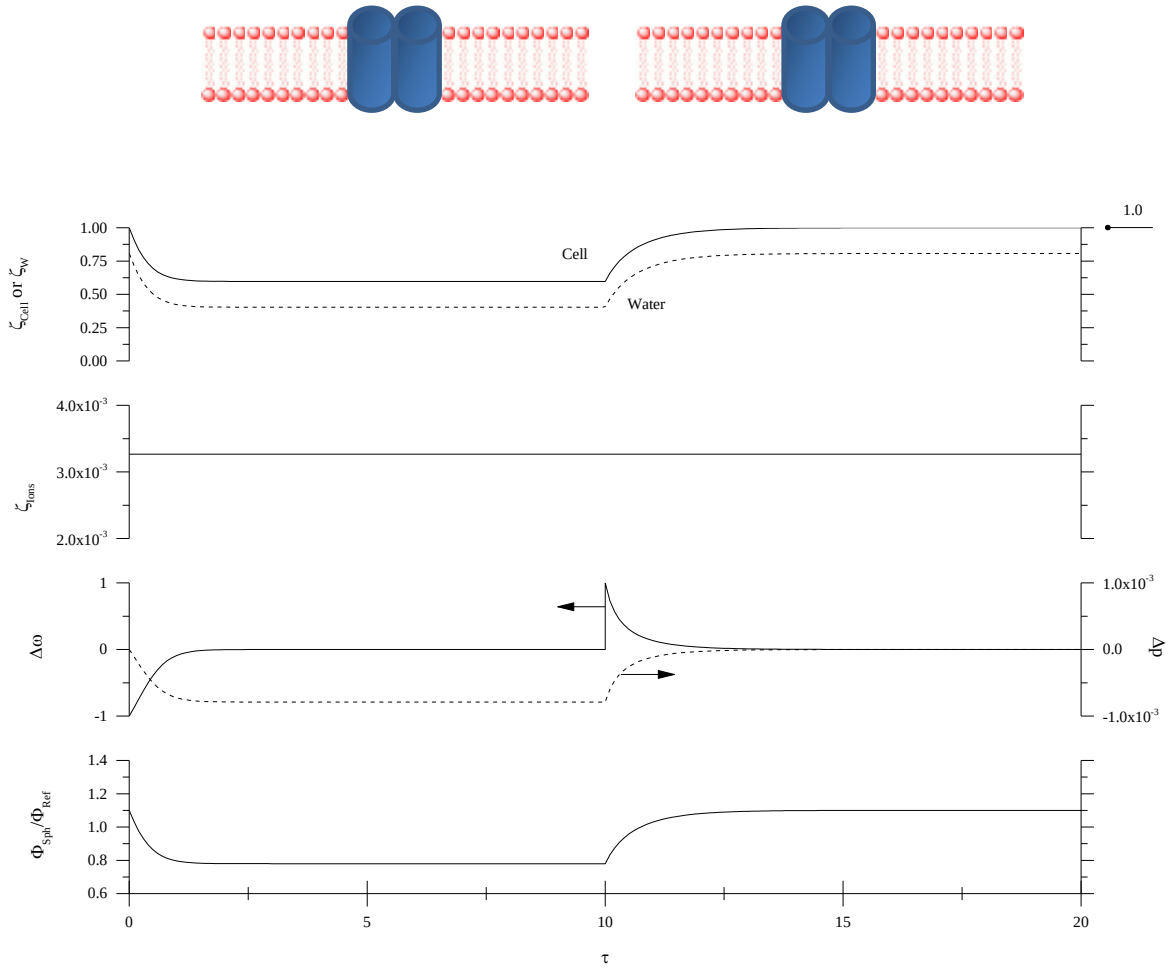

Figure 4: Osmotic cycle with impermeant sucrose in the absence of permeant CPA: results of the SAR model in the parameter sweep analysis with an infinitely slow membrane relaxation rate ($\lambda_S = 0$). The simulation of the two-parameter model is not reported because it does not change from Figure 2.

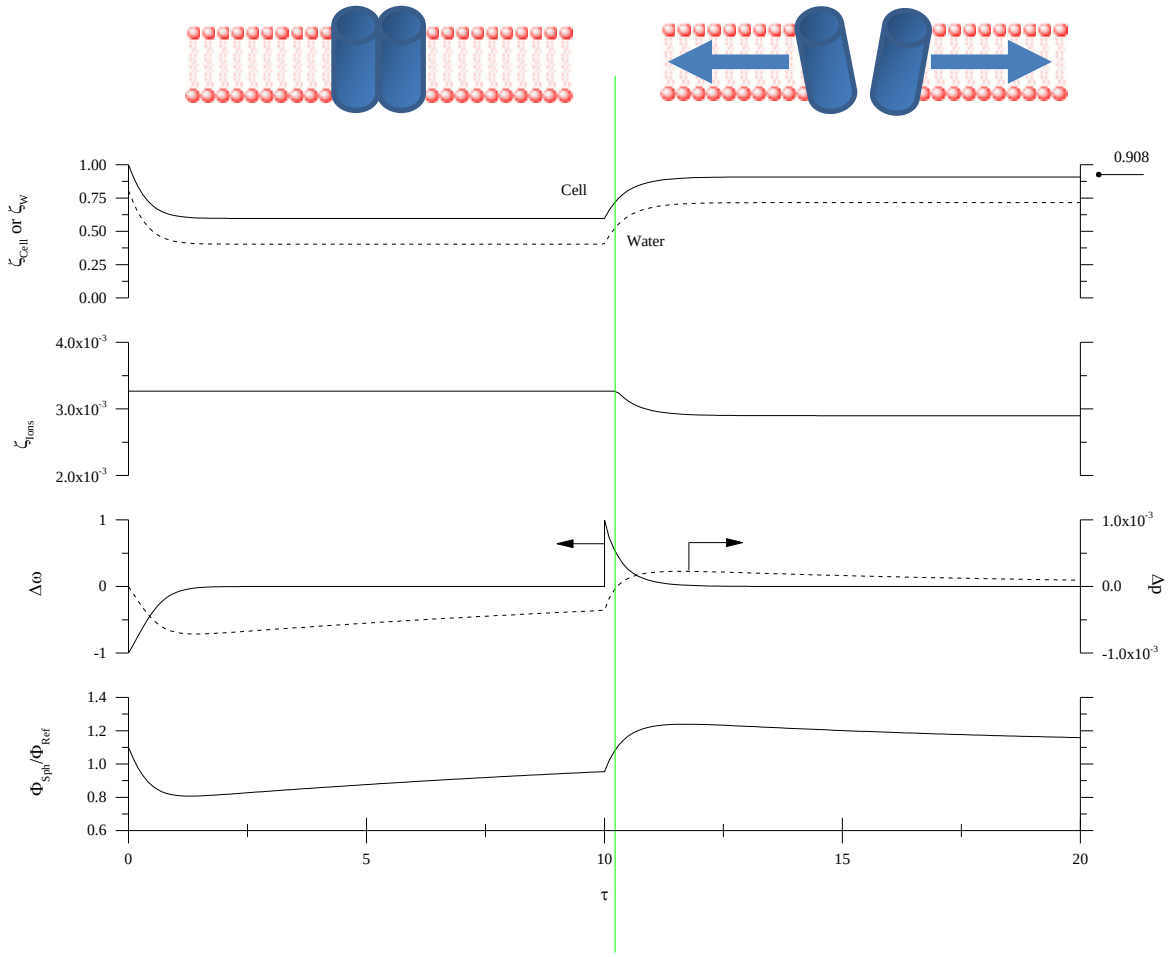

Figure 5: Osmotic cycle with impermeant sucrose in the absence of permeant CPA: results of the SAR model in the parameter sweep analysis with a membrane relaxation rate slower than in the base case ($\lambda_S = 8.42$). The vertical, green line represents the time of MS channels opening. The simulation of the two-parameter model is not reported because it does not change from Figure 2.

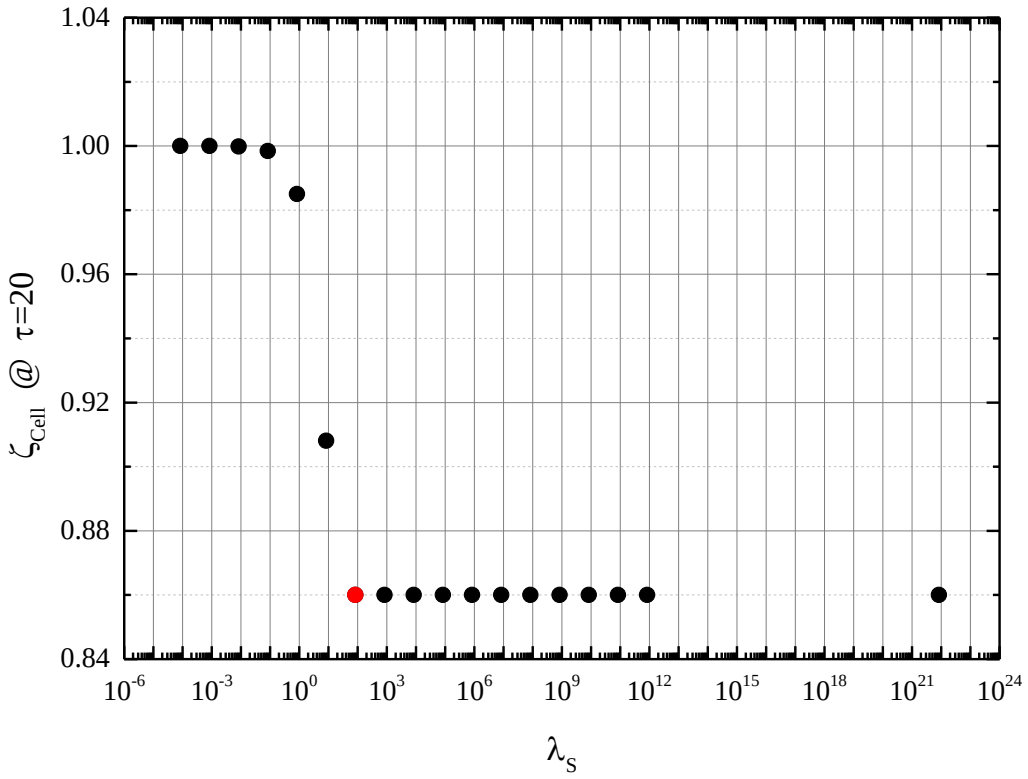

Figure 6: Osmotic cycle with impermeant sucrose in the absence of permeant CPA: results of the SAR model in terms of the cell volume at the end of phase II ($\zeta_{\mathrm{Cell}}\,@\,\tau = 20$) for the sweep of parameter λ_S (total duration of osmotic cycle is 20, i.e. 10 for both phase I and II); base case in red.

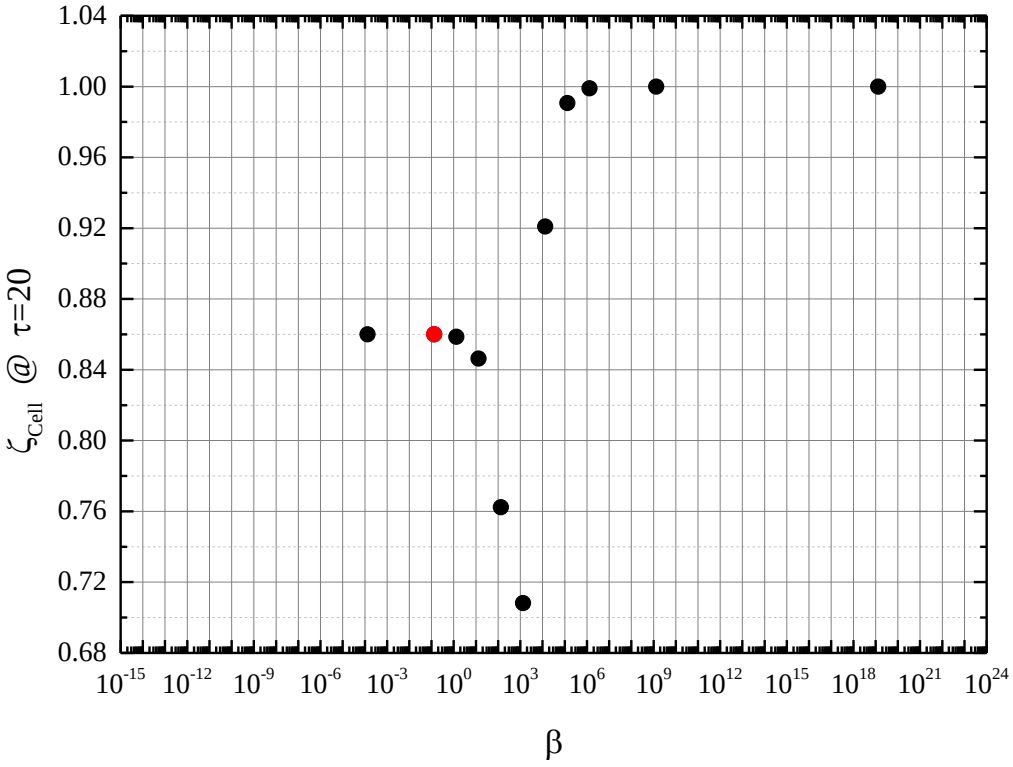

Figure 7: Osmotic cycle with impermeant sucrose in the absence of permeant CPA: results of the SAR model in terms of the cell volume at the end of phase II ($\zeta_{\mathrm{Cell}}\,@\,\tau = 20$) for the sweep of parameter β (total duration of osmotic cycle is 20, i.e. 10 for both phase I and II); base case in red.

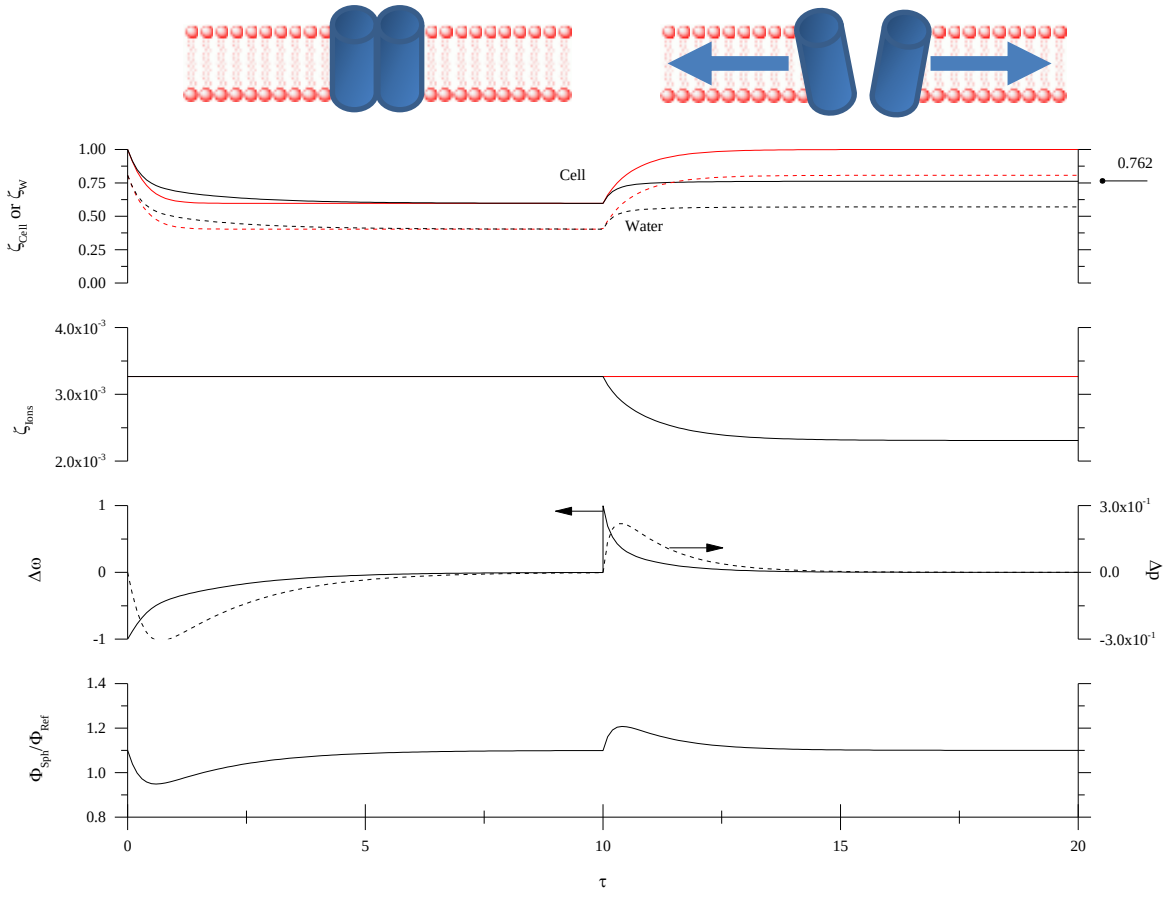

Figure 8: Osmotic cycle with impermeant sucrose in the absence of permeant CPA: comparisons between the results of the SAR model (black) and the two-parameter model (red) in the parameter sweep analysis with $\beta = 1.32 \cdot 10^2$, three orders of magnitude increase with respect to its base case value. The simulation of the two-parameter model is reported for convenience even though it does not change with respect to Figure 2.

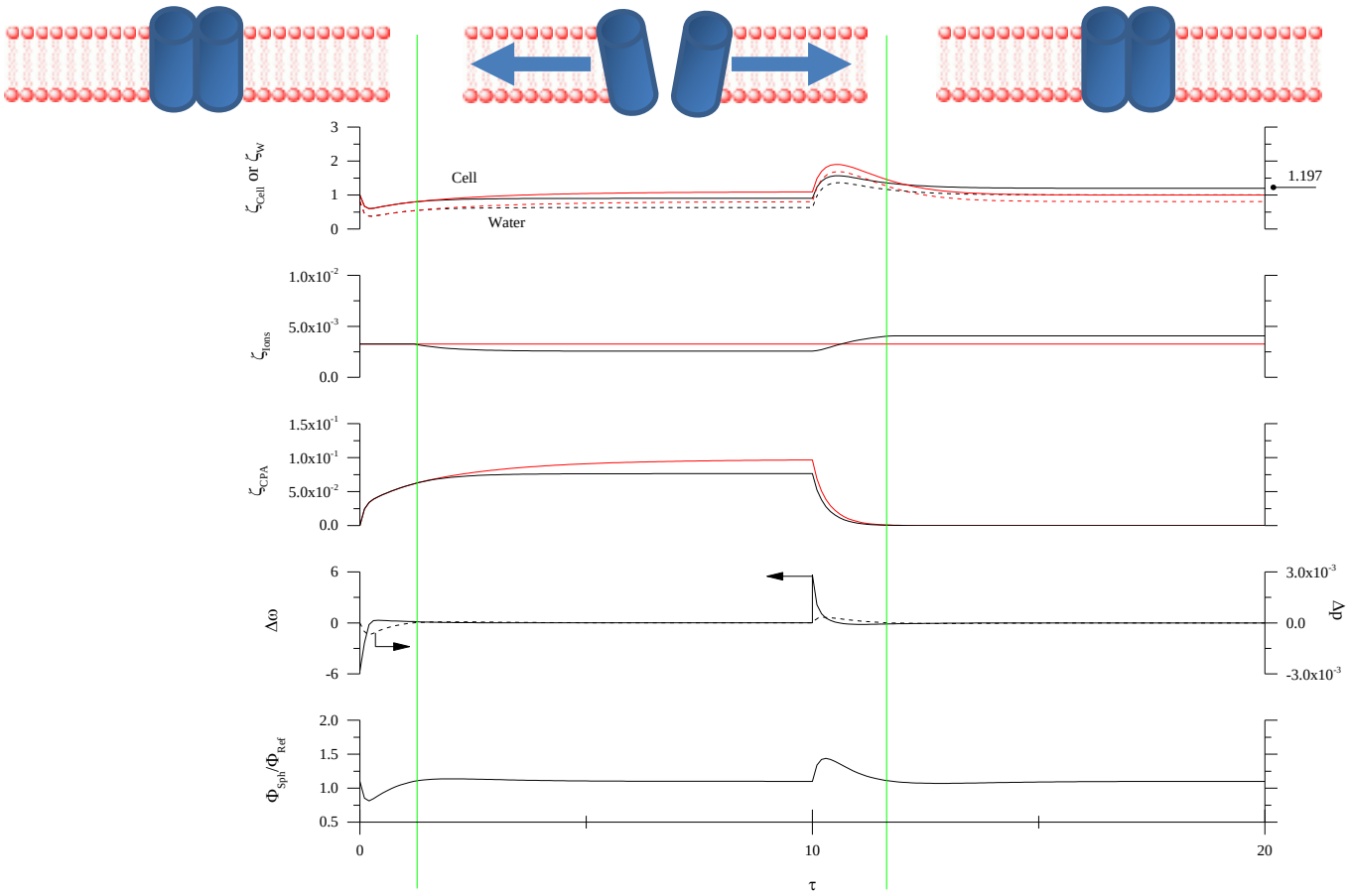

Figure 9: Osmotic cycle with permeant DMSO in the absence of impermeant sucrose: comparisons between the results of the SAR model (black) and the two-parameter model (red) using the parameter values reported in Table 4 (base case). The vertical, green lines indicate opening and closing of MS channels.

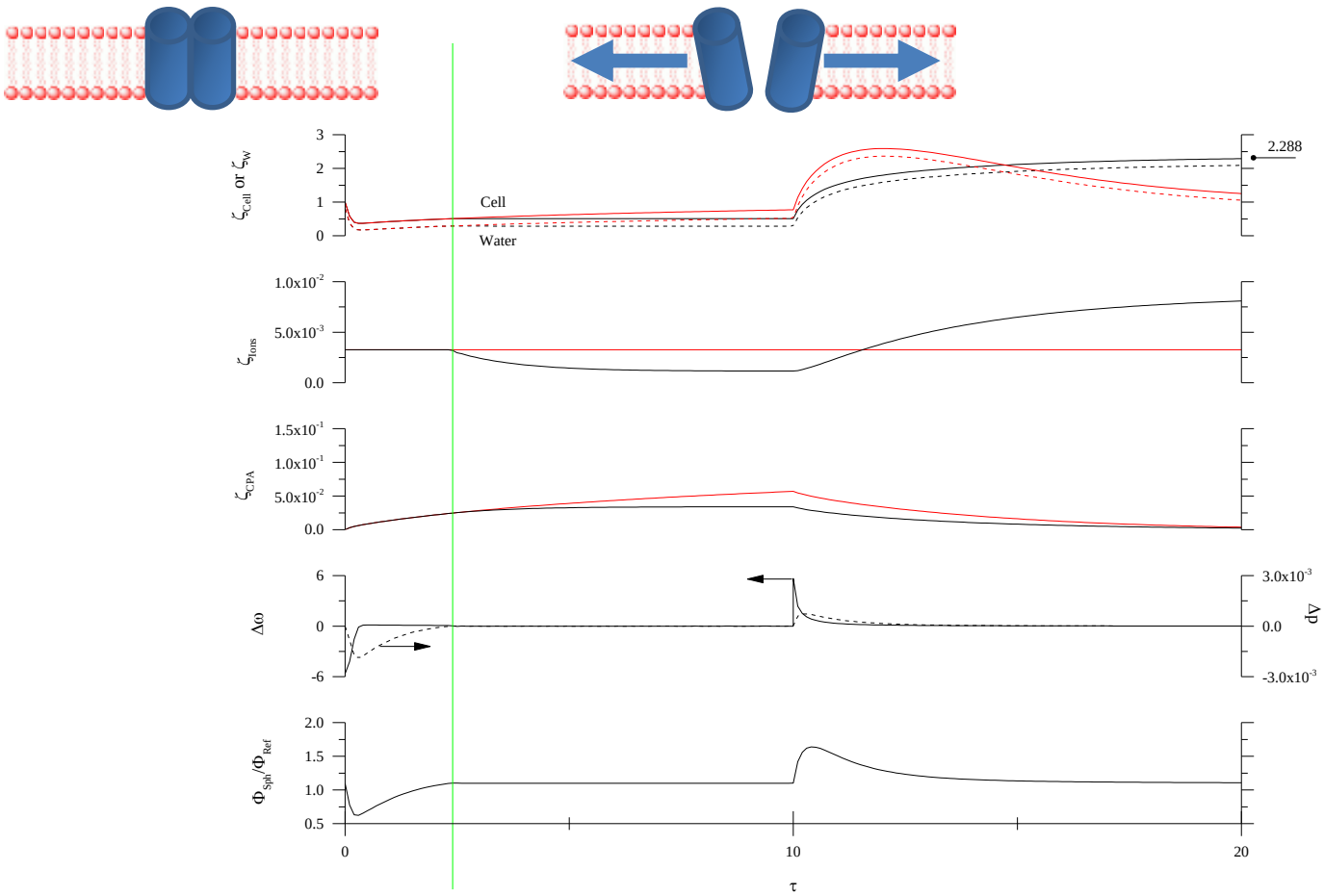

Figure 10: Osmotic cycle with permeant DMSO in the absence of impermeant sucrose: comparisons between the results of the SAR model (black) and the two-parameter model (red) in the parameter sweep analysis with $\lambda_{\mathrm{CPA}} = 6.26 \cdot 10^{-3}$, one order of magnitude decrease with respect to its base case value. The vertical, green line indicate opening of MS channels.

Captions for figures

Figure 1 Schematic representation of a cell according to the SAR model.

Figure 2 Osmotic cycle with impermeant sucrose in the absence of permeant CPA: comparisons between the results of the SAR model (black) and the two-parameter model (red) using the parameter values reported in Table 4 (base case).

Figure 3 Equilibrium conditions ($\zeta_{\mathrm{Cell}}^{\mathrm{I}}$ and $\zeta_{\mathrm{Cell}}^{\mathrm{II}}$) of the SAR model for the osmotic cycle with sucrose in the parametric sweep analysis: variation of ion permeability ($\lambda_{\mathrm{Ions}} = 1.07 \cdot 10^{-3}, 2.14 \cdot 10^{-3}, 1.07 \cdot 10^{-2}$), with base case in bold lines. Circles represent the corresponding numerical integration of the dynamic SAR model (ζ_{Cell} @ $\tau = 10$ and ζ_{Cell} @ $\tau = 20$).

Figure 4 Osmotic cycle with impermeant sucrose in the absence of permeant CPA: results of the SAR model in the parameter sweep analysis with an infinitely slow membrane relaxation rate ($\lambda_{\mathrm{S}} = 0$). The simulation of the two-parameter model is not reported because it does not change from Figure 2.

Figure 5 Osmotic cycle with impermeant sucrose in the absence of permeant CPA: results of the SAR model in the parameter sweep analysis with a membrane relaxation rate slower than in the base case ($\lambda_{\mathrm{S}} = 8.42$). The vertical, green line represents the time of MS channels opening. The simulation of the two-parameter model is not reported because it does not change from Figure 2.

Figure 6 Osmotic cycle with impermeant sucrose in the absence of permeant CPA: results of the SAR model in terms of the cell volume at the end of phase II (ζ_{Cell} @ $\tau = 20$) for the sweep of parameter λ_{S} (total duration of osmotic cycle is 20, i.e. 10 for both phase I and II); base case in red.

Figure 7 Osmotic cycle with impermeant sucrose in the absence of permeant CPA: results of the SAR model in terms of the cell volume at the end of phase II (ζ_{Cell} @ $\tau = 20$) for

the sweep of parameter β (total duration of osmotic cycle is 20, i.e. 10 for both phase I and II); base case in red.

Figure 8 Osmotic cycle with impermeant sucrose in the absence of permeant CPA: comparisons between the results of the SAR model (black) and the two-parameter model (red) in the parameter sweep analysis with $\beta = 1.32 \cdot 10^2$, three orders of magnitude increase with respect to its base case value. The simulation of the two-parameter model is reported for convenience even though it does not change with respect to Figure 2.

Figure 9 Osmotic cycle with permeant DMSO in the absence of impermeant sucrose: comparisons between the results of the SAR model (black) and the two-parameter model (red) using the parameter values reported in Table 4 (base case). The vertical, green lines indicate opening and closing of MS channels.

Figure 10 Osmotic cycle with permeant DMSO in the absence of impermeant sucrose: comparisons between the results of the SAR model (black) and the two-parameter model (red) in the parameter sweep analysis with $\lambda_{\mathrm{CPA}} = 6.26 \cdot 10^{-3}$, one order of magnitude decrease with respect to its base case value. The vertical, green line indicate opening of MS channels.